

## Article

# Technoeconomic Analysis of Intensified PEGylated Biopharmaceutical Recombinant Protein Production: Alpha Antitrypsin as a Model Case

Salem Alkanaimsh <sup>\*</sup>, Abdullah M. Alsalam  and Hesham El-Touney

Department of Chemical Engineering, College of Engineering and Petroleum, Kuwait University, P.O. Box 5969, Safat, Kuwait City 13060, Kuwait; abdullah.alsalam@ku.edu.kw (A.M.A.); hisham.ettouney@ku.edu.kw (H.E.-T.)

\* Correspondence: s.alkanaimsh@ku.edu.kw; Tel.: +965-24985617

**Abstract:** Alpha-1 antitrypsin deficiency (AATD) is a genetic disorder characterized by the insufficient production of the AAT protein. Due to availability limitations, not all AATD patients receive protein therapy treatment. In this study, the technoeconomic analysis of different processes (conventional and intensified) producing 200 kg/year of PEGylated recombinant AAT (PEG-AAT) using a Chinese hamster ovary cell line was investigated. All bioprocesses consist of upstream, downstream, and PEGylation sections. A base-case model (process A) of the conventional fed-batch production bioreactor was developed using SuperPro Designer software (Version 13) to evaluate the economic feasibility of the process. The cost of goods (COG) was estimated to be approximately USD 387.6/g. Furthermore, an intensified process (B) was modeled and evaluated to reduce the COG. Process intensification was implemented in the process (N-1 perfusion bioreactor). The specific operating COG for process B was found to be 10% less than that of process A. Scenario analysis was performed to assess the impact of process capacity (100–1000 kg/year) and cell-specific productivity (30–90 pg/cell/day). With an increase in process capacity, the specific operating COG was reduced for all processes. Increasing cell-specific productivity decreases the specific operating COG at different rates for each process, depending on the titer level. Future investigations into the PEGylation section are required since it has the highest COG of all the sections.



**Citation:** Alkanaimsh, S.; Alsalam, A.M.; El-Touney, H. Technoeconomic Analysis of Intensified PEGylated Biopharmaceutical Recombinant Protein Production: Alpha Antitrypsin as a Model Case. *Processes* **2024**, *12*, 979. <https://doi.org/10.3390/pr12050979>

Academic Editor: Ravendra Singh

Received: 1 April 2024

Revised: 3 May 2024

Accepted: 7 May 2024

Published: 10 May 2024



**Copyright:** © 2024 by the authors. Licensee MDPI, Basel, Switzerland. This article is an open access article distributed under the terms and conditions of the Creative Commons Attribution (CC BY) license (<https://creativecommons.org/licenses/by/4.0/>).

**Keywords:** technoeconomic analysis; protein PEGylation; process intensification; scenario analysis; bioprocess engineering

## 1. Introduction

Alpha antitrypsin is a well-known member of the serine protease inhibitor (SERPIN) superfamily. Its primary function is to protect tissue from serine proteases released during inflammation, including neutrophil elastase and proteinase 3 [1]. Moreover, it has the ability to neutralize other proteases like cysteine proteinases and metalloproteases [2]. AAT protein is produced and secreted into the serum by hepatocytes with a mean concentration of 1–2 g/L. Its mature form consists of nine alpha helices, three beta sheets, and a reactive center loop (RCL), which form the initial interaction with the target protease during inhibition [3,4]. AAT consists of 394 amino acid residues (~52 kDa), of which three N-glycosylation sites are located at positions Asn-46, Asn-83, and Asn-247. The total carbohydrate mass is roughly 15% that of the mature protein [5]. Strongly affected by glycosylation, the serum half-life of AAT protein is 4–5 days [6].

As a key player in the protease–antiprotease balance in the lung, AAT protein is the chief antiprotease ensuring lung homeostasis. If this balance is disturbed, an excess of protease causes inflammatory damage in the lung tissue, as seen in a number of viral infection diseases [7,8]. Furthermore, this imbalance involves the progression of a number of chronic diseases, such as chronic obstructive pulmonary disease (COPD) and emphysema [9]. On

the genetic level, AATD is one of the major causes of COPD [10]. AATD is caused by point mutations in the amino acid sequence of mature alpha antitrypsin protein, resulting in lower circulating alpha antitrypsin in serum. The most clinically relevant mutants are S (E264V) and Z (E342K). The names of these mutants are associated with their mobility in isoelectric focusing: S is slow and Z is very slow relative to normal AAT [11,12]. The serum AAT level associated with milder AATD genotypes ranges from 1–1.8 g/L to 0.45–0.8 g/L, depending on the AATD genotype [13].

Homozygotes for the Z allele corresponding to patients with a serum level of AAT at about 10% of the normal serum level are the most severe forms of AATD [14]. This level is below the threshold needed for protection of 11  $\mu$ M [15]. In order to determine the magnitude and distribution of AATD, several publications have estimated the prevalence of PiZ allele mutation and PiZZ homozygous mutation worldwide. For example, Blanco et al. estimated that there are roughly 250,000 patients with the PiZZ homozygous mutation worldwide, half of whom are in Europe [16]. Thus, developing therapeutics for AATD is a necessity and an unmet need.

Different therapeutic approaches for the treatment of lung and liver diseases associated with AATD have been proposed in the literature, as summarized by McElvaney et al. [17]. Augmentation with plasma-derived authentic AAT remains the only approved treatment for AATD-related lung disease. The management protocol for the disease currently consists of life-long augmentation therapy with weekly infusions of 60 mg AAT/kg body weight [18–20]. Although authentic human AAT has been purified to a great extent from human plasma and Cohn fraction IV [2], limited resources for authentic human AAT from plasma or its derivatives make this process unsustainable. For example, in the U.S., only 5000 severely deficient patients out of an estimated 60,000 PiZZ carriers receive a weekly dose based on the required amount mentioned earlier [5,16]. Thus, the development of recombinant-form AAT not only helps to expand the number of severely deficient recipients receiving treatments but also helps to reduce the risk of blood-prone pathogen transmission and lower production costs [18].

Immortalized Chinese hamster ovary cells (CHO cells) represent an attractive tool for the production of the vast majority of recombinant protein therapeutics (~70%), including monoclonal antibodies [21]. Recombinant AAT is no exception, as CHO cells are capable of producing recombinant AAT at high titers [22]. Moreover, the ability to engineer cell lines or the protein to have superior properties compared to authentic human AAT makes the production platform attractive [23–25]. Traditionally, production bioreactors are operated in fed-batch mode due to their operational simplicity, high product yield, and reproducibility and scalability [26,27]. Nonetheless, fed-batch production processes require large-volume bioreactors to meet demand. To meet biopharmaceutical protein demand, process intensification stands as a tool to reduce the footprint, decrease the capital cost, and improve productivity. As described by Chen et al., it stands for a collection of efforts to increase the volumetric productivity of the bioprocess by either increasing cell-specific productivity, increasing viable cell density, or decreasing the non-productive stages of the culture through the combined effects of media optimization, cell engineering, or increasing seed cell density [28]. For example, Xu et al. showed an increase in product titer and an order-of-magnitude decrease in COG for monoclonal antibody products when comparing conventional processes relative to hybrid intensified processes that involved process intensification at the seed culture step (N-1) and the continuous downstream process [29,30]. Müller et al. showed that N-1 perfusion used as an upstream process intensification approach to feed a high-seed fed-batch bioreactor was able to increase volumetric productivity by a two-fold increase due to a 50% increase in protein titer and by shortening the process from 14 days to only 10 days [31]. Therefore, process intensification is a valuable approach to reducing the bioreactor's size and enhancing the economic metrics of the bioprocess (total capital cost (CAPEX, USD), the annual operating cost (OPEX, USD/year), and the unit production cost (cost of goods (COG), USD/g), as demonstrated in recent bioprocess techno-economic modeling articles [32–35].

One of the inherited limitations of CHO cell culture is the sialylation extent of the N-glycans of recombinant proteins, which is known to have a beneficial effect on the half-life of therapeutic proteins [36,37]. For example, Raymond et al. reported that the synergic effect of Fc mutation (F243A) and co-expression of  $\beta$  1,4-galactosyltransferase 1 and  $\alpha$ 2,6-sialyltransferase 1 was necessary to boost the percentage of sialylated N-glycans in the Fc region of humanized trastuzumab. The percentage changed from <1% for the wild-type case with no co-expression of glycosyltransferases to greater than 75% upon Fc mutation and the co-expression of glycosyltransferases [38]. One of the technologies to increase the protein half-life is PEGylation, which is a covalent conjugation of polyethylene glycol polymer to amino acid residues, causing the protein to have improved physiochemical properties as well as an increase in size and retention in the body [39]. It is a widely used therapeutic approach; there are more than 25 FDA-approved PEGylated recombinant protein drugs on the market [40]. Although random PEGylation (covalent attachment to lysine residue) is the route to producing PEGylated protein therapeutics for most approved drugs, random PEGylation suffers from creating PEGmers (monoPEGylated, diPEGylated, and triPEGylated species). Moreover, producing positional isomers is possible due to the different reactivities of lysine residues, leading to pharmacologic, toxicologic, and immunogenic activities [41]. On the other hand, site-specific PEGylation is more desirable in order to avoid creating multiple PEGmers [42]. Since cysteine accounts for roughly 1% of the amino acid residues in proteins, it represents an attractive option for bioconjugation, especially if the proteins have free cysteine, which is not involved in disulfide bond formation [43]. Since alpha antitrypsin has a single cysteine, it is an ideal bioconjugation site for PEGylation, as shown by different research groups using either authentic human AAT or recombinant forms of AAT [44–46].

This article presents a techno-economic simulation model of a hypothetical plant facility aiming at producing PEGylated recombinant AAT protein. The process is divided into three sections: the upstream section, the downstream section, and the PEGylation section. A process simulation using SuperPro Designer software (Version 13) was developed and run to perform a manufacturing cost analysis for the base case process (process A), aiming at a production level of 200 kg PEGylated AAT/year. The total capital cost (CAPEX, USD) and the annual operating cost (OPEX, USD/year) that includes facility-dependent cost, material and consumables cost, labor cost, and unit production cost (cost of goods (COG) USD/g) were analyzed. Moreover, an alternative intensified process (process B) that uses elements of process intensification at the seed culture step (N-1) to increase seed cell density in the production bioreactor was constructed and compared to the conventional process in terms of CAPEX, OPEX, and COG. Furthermore, alternative facilities were simulated by varying the production titer (i.e., varying cell-specific productivity) and production capacity at a fixed production titer for each process. The COG of each alternative bioprocess was compared to the base case with respect to its constituents (i.e., facility-dependent cost, material and consumables cost, and labor cost). To the knowledge of the authors, no previous study has discussed the techno-economic modeling of intensified processes aiming to produce PEGylated recombinant protein.

Although hypothetical, the simulated facility is based on generally accepted bioprocess engineering design principles or parameters that are related to AAT. For example, in the upstream section, the cell-specific productivity is based on Chin et al., who showed that AAT productivity could go as high as 90 pg/cell/day using selection stringency on expression vectors for the production of AAT [22]. A cell productivity of 30 pg/cell/day was assumed. Furthermore, the doubling time was in the range of 30–45 h. Growth rates of  $0.37 \text{ day}^{-1}$  (doubling time 45 h) were assumed in the production bioreactor in the conventional process A, while a lower growth rate of  $0.2 \text{ day}^{-1}$  was assumed in the intensified process B, which is a consequence of high cell seed density [30,47,48]. Moreover, the feeding rate in the production bioreactor and the perfusion rate in the perfusion bioreactor, as well as the starting seed density of conventional and intensified bioprocesses, are within the general design parameters of CHO-based bioprocesses [29,30,48]. Furthermore, the selection of

capture affinity chromatography [49] and orthogonal chromatography polishing steps to remove impurities such as host DNA and residual host cell proteins (HCP) related to AAT is widely used and resembles a conventional downstream step in bioprocesses [50,51]. The choice of appropriate buffers used in cyclic operations of different chromatography unit operations is based on the literature. Additionally, filtrate flux in tangential flow filtration unit operations applied for diafiltration or concentrating protein solution is selected based on manufacturing instructions [52]. Finally, the operating conditions in the PEGylation reactor (i.e., reaction buffer's pH and temperature), the kinetic parameters constants used to evaluate the time to achieve a specific yield of PEG-AAT, and the operating conditions of chromatography unit operation to separate PEG-AAT from AAT were extracted from the literature [44,53].

## 2. Materials and Methods

### 2.1. Process Description

Traditionally, biopharmaceutical manufacturing for protein therapeutics contains the following sections: the upstream process, which includes inoculation, media preparation, seed culture expansion, and protein production; and the downstream process, which includes clarification, primary capture, and polishing. However, in our process, an extra section, protein PEGylation, is introduced. Inoculation is applied to the scale-up cell culture. Usually, it takes place in a series: shake flask, wave bioreactor, and stirred seed culture bioreactor (stainless steel or single-use). The production bioreactor begins with a certain viability and density from the seed train. The bioreactor runs at 36.5 °C with a dissolved oxygen level of 40%.

Two different processes were modeled that share the same downstream processing and PEGylation sections. They differ in upstream processes (conventional and intensified). In the conventional process (process A), seed expansion occurs in a series of Erlenmeyer flasks, wave bioreactors (50 L and 200 L), and seed N-1 single-use bioreactors (500 L). The wave bioreactors, N-1 seed bioreactors, and N-production bioreactors are associated with auxiliary equipment to prepare, filter, and sterilize the media. Moreover, air filters are modeled to be used in conjunction with N-1 seed bioreactors and N-bioreactors. The final cell density after the N-1 bioreactor is  $4.0 \times 10^6$  cells/mL, and the expansion duration is roughly 17 days from the shake flasks to the N-1 seed bioreactor, based on a growth rate of  $0.62 \text{ day}^{-1}$ . A seed inoculum density of  $0.2 \times 10^6$  cells/mL is assumed. The capacity of the production bioreactor is 2000 L, with a 62% initial capacity. The cells are allowed to grow to reach a viable cell density of  $1.8 \times 10^6$  cells/mL before being fed a solution of concentrated glucose and amino acids. In our process (process A), feeding was conducted daily with a 3% preceding volume present in the vessel for a total duration of 14 days, where the final cell density reached  $5.1 \times 10^6$  cells/mL. The production bioreactor was modeled by having four different phases during the production, namely, the batch exponential phase, the exponential phase with feeding, the stationary phase, and the death phase. Cell-specific productivity was assumed at 30 pg/cell/day based on the number of Chin et al. [22] in order to solve the ordinary differential equations of the production N-bioreactor, as shown in the Supplementary Information (Equations (S1)–(S21)); a more detailed explanation is included in Section 2.4, and the titer level was calculated. The main assumptions of the N-bioreactor are shown in Table S1. The titer level was calculated at a level of 1.5 g/L. Based on the annual production capacity of 200 kg PEG-AAT/year and the AAT protein titer of 1.5 g/L, four N-production bioreactors ( $V = 2000$  L) were modeled. Based on the model, the amount of AAT protein per batch is 9.6 kg, and the total number of batches is 21/year.

The downstream process started with a centrifuge to remove the cell biomass from the supernatant. The supernatant, which contained the primary target protein (AAT) and HCP, was filtered to protect the primary capture affinity resin. The filtered supernatant was sent to the primary capture step, which was selectively bound to the AAT protein [49,54]. Based on the supplier's information, the resin capacity is 10 g AAT/L resin. Due to the

limited binding capacity and large amount of supernatant after filtration ( $V = 7570$  L), the column ran in multiple cycles (resin volume was 500 L, which means that the number of cycles was 3, assuming a linear velocity of 150 cm/h). Phosphate-buffered saline was used as an equilibration buffer and wash buffer to remove the non-bound proteins from the resin after loading the sample. The elution buffer was a concentrated 2 M  $MgCl_2$  solution that disturbed the binding of the AAT and the ligand. The protein yield from this operation was assumed to be 90% based on the loss of proteins during capture affinity chromatography. The following step was diafiltration, where the protein solution was concentrated (2-fold), and excess salt used in protein elution was removed using tangential flow filtration. The tangential flow filtration was modeled, assuming it was operated at a flux of 50 L/m<sup>2</sup>/h. Multiple diafiltration volumes (15) of phosphate buffer were passed to exchange the buffer for phosphate buffer. Diafiltration was followed by viral inactivation (solvent/detergent rather than low pH [55–57]) by holding the purified protein solution in a storage tank. Polishing steps (anion exchange chromatography and hydrophobic interaction chromatography) were used to remove residual impurities such as HCP and DNA [50,58], and they were used in the downstream processing of human authentic and recombinant AAT [51,59]. Q-Sepharose ( $V = 90$  L) was used as the anion exchanger in the B/E mode and was used primarily to remove DNA and HCP. Assuming a linear velocity of 150 cm/h, the number of cycles per batch was 2. The following polishing step was the HIC membrane adsorber in run in flow-through mode. The collected pure AAT fractions from the anion exchanger were mixed with ammonium sulfate to reach a concentration of 0.8 M. This concentration was assumed based on the work of Fan et al. in order to decrease the hydrophobicity of the AAT and prevent its binding to the membrane adsorber [51]. Diafiltration to exchange the protein's buffer was employed (flux = 50 L/m<sup>2</sup>/h) to concentrate the pure collected AAT and to exchange the buffer into saline phosphate buffer by passing the 15 diafiltration volume. The resulting pure AAT protein solution was set at a concentration of 50 g/L in appropriate conditions (alkaline saline buffer) for the PEGylation reaction section. The overall yield of the downstream processing was 77%, which is close to alpha antitrypsin purification yields obtained using immunosorbents [60].

The PEGylation reaction section consisted of a reactor vessel and a TFF diafiltration step to prepare the solution for subsequent ion exchange chromatography. A second diafiltration step was used to change the buffer and concentrate the derivative PEGylated AAT protein. Based on the findings of Liu et al. [44], the yield of PEGylated AAT protein was 66% when the reaction was run for 60 min at pH 7, and the initial molar ratio of PEG/AAT was 4:1. A theoretical yield of 100% was not achievable, as PEG-maleimide is known for being susceptible to hydrolysis in aqueous buffers [61]. The initial concentration of AAT was 20 g/L after diluting the pure AAT sample from the downstream section with reaction buffer (alkaline phosphate saline buffer), while the initial molar concentration of PEG/AAT was 10:1. Based on the deactivation constant of the PEG-maleimide reagent [53], a 92% yield was estimated, as shown in the Supporting Information, by solving the ordinary differential equation for the batch reactor (Equations (S22) and (S23) after allowing the reaction to proceed for 90 min). The reaction mixture was sent to a diafiltration (TFF) unit to lower the salt for subsequent chromatography unit operation anion exchange chromatography (Q-Sepharose). Similar to the earlier TFF unit operations, a 50 L/m<sup>2</sup>/h flux was assumed. The stream after the PEGylation batch reactor was concentrated 2-fold, and 10 diafiltration volumes were passed. Anion exchange chromatography was modeled as a subsequent unit operation to purify PEG-AAT in B/E mode, which resulted in a yield of 88%. Finally, the pure PEG-AAT was concentrated, and the buffer was exchanged for phosphate-buffered saline by operating at a flux of 50 L/m<sup>2</sup>/h. The resulting PEG-AAT concentration was 15 g/L, with purity exceeding 99%.

Regarding the intensified process, process B was assumed to have an inoculum density of  $8 \times 10^6$  cells/mL in the N-bioreactor. In order to reach such a high cell density, the N-1 perfusion bioreactor was assumed to run at a perfusion rate of 0.04 nL/cell/day to increase

the seed biomass from  $5.0 \times 10^6$  to  $84 \times 10^6$  cells/mL after 7 days of operation. A similar operational procedure and cell-specific productivity (30 pg/cell/day) were assumed in the N-bioreactor in the intensified process. Based on the assumptions listed in Table S1 and with the aid of ordinary differential equations of the production bioreactor (Equations (S1)–(S21)), the titer level was calculated at a level of 3.5 g/L.

The volumes of the N-1 and N-production bioreactors were adjusted so that the amount of AAT protein produced per batch and, thus, the annual production level of PEG-AAT stayed the same across both processes. For example, process B had two N-1 200 L seed wave bioreactors and two 2000 L N-production bioreactors. On the other hand, process A had a single 500 L N-1 seed bioreactor and four 2000 L production N-bioreactors. Altogether, the production level of AAT per batch stayed at a level of 9.6 kg per batch, and all processes were scheduled to have 21 batches annually to produce the 200 kg PEG-AAT. The downstream and PEGylation sections of the intensified process B were mostly the same compared to those of conventional process A, except for the duration of the centrifuge and capture chromatography, which depend on the volume of the production N-bioreactor. Nonetheless, the duration difference has a negligible effect on the total annual number of batches.

The yield of the downstream and PEGylation sections is summarized in Table S2. Figures 1–3 provide the process operation for process A in the upstream, downstream, and PEGylation sections, respectively. On the other hand, Figure S1 provides the upstream process operation for process B.

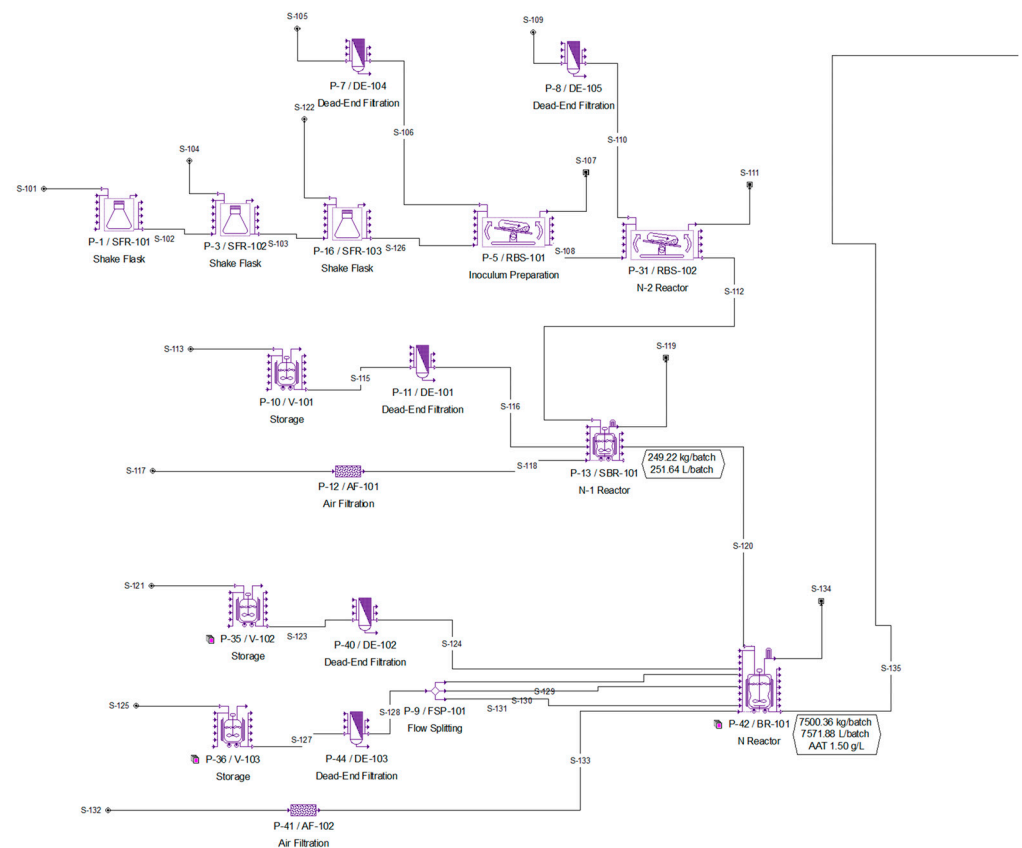


Figure 1. Process flow diagram of the upstream section of conventional process A.

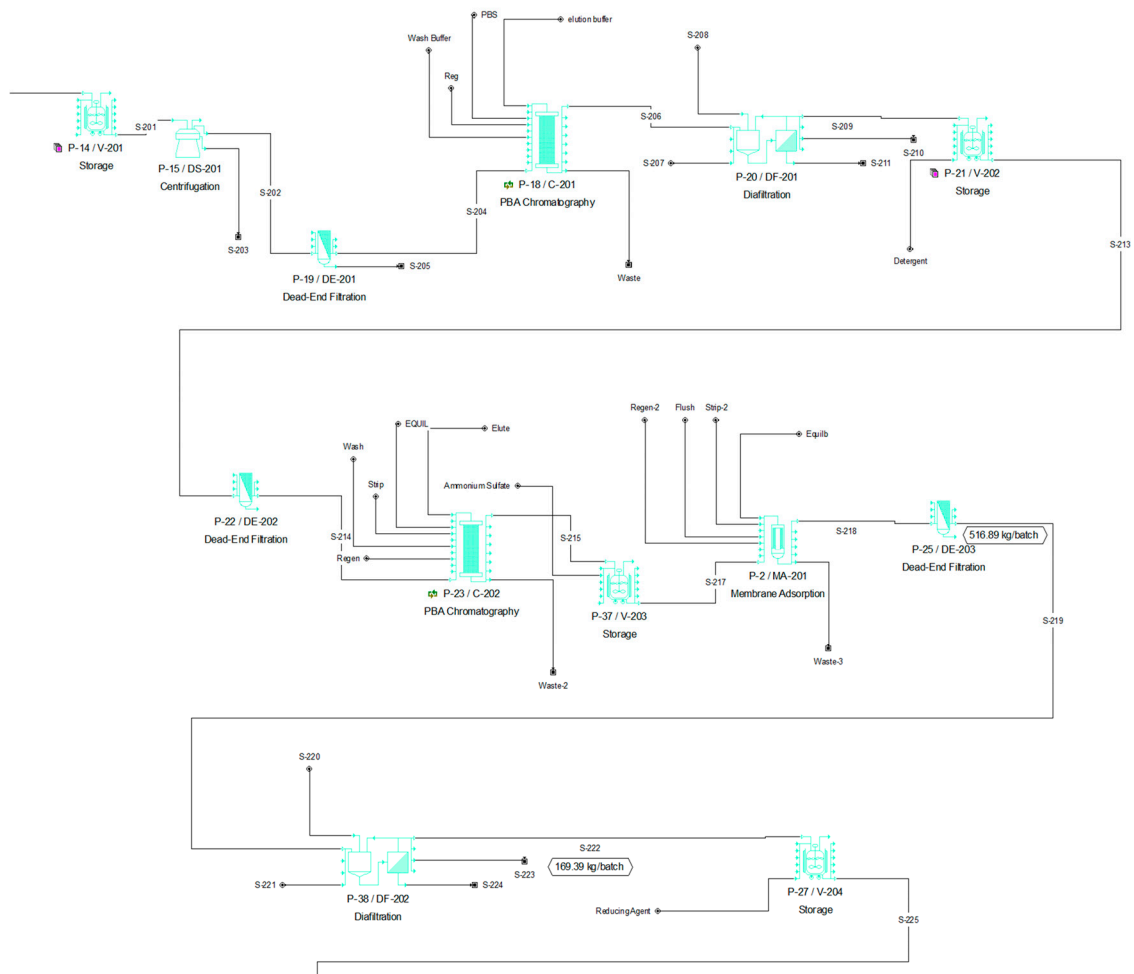


Figure 2. Process flow diagram of the downstream section of conventional process A.

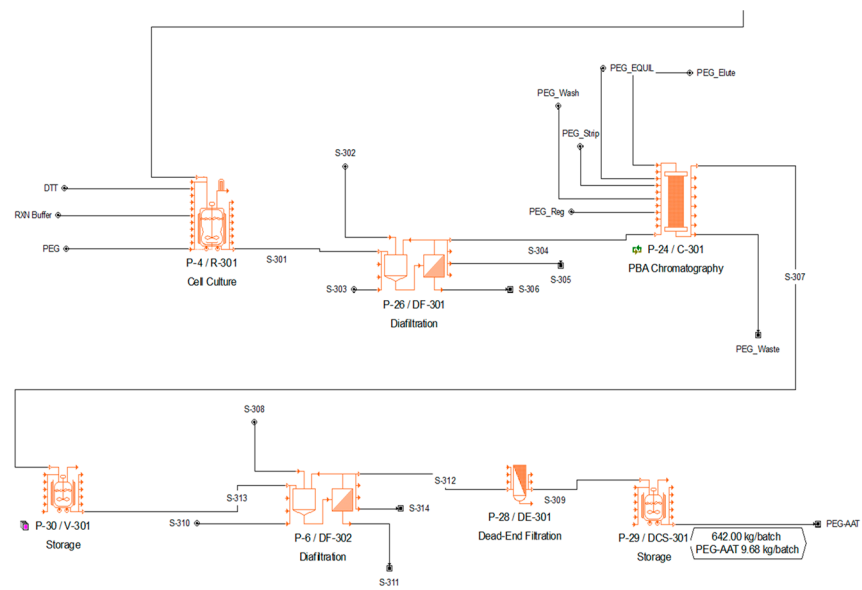


Figure 3. Process flow diagram of the PEGylation section of conventional process A.

## 2.2. Economic Analysis and Process Simulation

The production expenditure consists of the total capital cost (CAPEX) and total annual operating cost (OPEX), which are similar to what is reported in the literature [33,34]. CAPEX and OPEX determine COG, which is defined as shown in Equation (1).

$$\text{COG} \left( \frac{\text{USD}}{\text{g}} \right) = \frac{\frac{\text{CAPEX}}{\text{Years of Operation}} \left( \frac{\text{USD}}{\text{year}} \right) + \text{OPEX} \left( \frac{\text{USD}}{\text{year}} \right)}{\text{Annual Production} \left( \frac{\text{g}}{\text{year}} \right)} \quad (1)$$

The selling price of the derivative PEG-AAT was assumed to be 500 USD/g, which is similar to the price of different authentic human AAT formulations, as reported by McNulty et al. [5]. All process simulations were performed using SuperPro Design Version 13 (Intelligen Inc., Freehold, NJ, USA), where different tasks can be set in a sequence for each unit operation. The software is capable of providing equipment occupancy charts and Gantt charts, among other features, after solving the material and energy balances of the process. Furthermore, economic analysis, such as an analysis of COG, can be performed. Equipment occupancy and Gantt charts for process A are shown in Figures S2 and S3, respectively. On the other hand, the equipment occupancy and Gantt charts for process B are shown in Figures S4 and S5, respectively.

## 2.3. Scenario Analysis

In order to investigate the impact of changing several process parameters on the process economics for all three processes, a scenario analysis was performed. In our model, the capacity of the plant for the two processes varied from 100 kg/year up to 1000 kg/year (the base case is 200 kg/year). Furthermore, cell-specific productivity was varied for each process from 30 pg/cell/day up to 90 pg/cell/day [22]. The COG was calculated and compared to the base case.

## 2.4. Bioreactors Mathematical Model

Each phase in the fed-batch operated production bioreactor was modeled to estimate the cell biomass and AAT protein concentration (batch phase: Equations (S1)–(S4), fed-batch: (S5)–(S12), stationary phase: (S13)–(S16), and death phase: (S17)–(S21)). In the batch phase, the volume of the media is assumed to be constant, and the biomass concentration increases exponentially over time, as shown in (S2). Making protein mass balance in the bioreactor enables solving for the increase in product mass over the batch period, as shown in (S4).  $X_0$ ,  $V_0$ ,  $q_p$ ,  $\mu$ ,  $X$ , and  $\Delta m$  represent the seed cell density (cell/mL), the initial volume (L), cell-specific productivity (pg/cell/day), growth rate ( $\text{day}^{-1}$ ), cell biomass as a function of time (cell/mL), and the product mass (kg), respectively. In the fed-batch phase, feeding is assumed to happen on a daily basis, with feeding assumed to occur at a percentage of the preceding volume present in the vessel ( $b$ ). Based on this feeding program, the volume increase can be calculated as a function of time, as shown in (S7). Subsequently, the biomass growth and product mass increase in the bioreactor can be found as shown in (S10) and (S12), respectively.  $F$ ,  $V$ , and  $b$  represent the flow rate in the vessel (L/day), the volume as a function of time (L), and the percentage of feeding flow relative to the preceding volume in the bioreactor ( $-$ ), respectively. In the stationary phase, the biomass cell concentration is assumed to be constant and reach maximum cell density (S13), and the product mass concentration is calculated as in the preceding phase. In the death phase, the death constant ( $k_d$ ;  $\text{day}^{-1}$ ) is assumed for each process and used to estimate the decline in the biomass, as shown in (S19). The product mass is calculated, as shown in (S21).

As for the PEGylation reactor, the kinetics of conjugation are assumed to follow elementary kinetics, as shown in (S22), where  $k$ ,  $C_{AAT}$ ,  $C_{PEG}$  represent the rate constant (L/mol/h), the concentration of AAT (M), and the concentration of PEG-maleimide reagent, respectively. Since the PEG-maleimide reagent is susceptible to deactivation in aqueous conditions, the kinetics of decreased concentration of PEG-maleimide reagent in the reactor

are affected by both first-order deactivation and elementary conjugation, represented by  $k_d$  ( $\text{h}^{-1}$ ), and conjugation reaction, represented by  $k$  ( $\text{L}/\text{mol}/\text{h}$ ).

### 3. Results and Discussion

#### 3.1. Economic Analysis

As described by Müller et al., process intensification is a key trend in biopharmaceutical manufacturing that aims to increase process efficiency and lower COG with different approaches that can be utilized in upstream or downstream components of the bioprocess [31]. This is a concept that is based on step-change improvements in technology, resulting in an increase not only in productivity but also in footprint and economic metrics (i.e., CAPEX and OPEX) [62]. Economic metrics of processes are measured using “technoeconomic analysis”, which is an analysis that aims to provide a combination of process simulations and cash flow analysis to estimate mass/energy balance and economic metrics of processes that can be used to check the viability of processes before commercialization [63,64]. Principles of process intensification have been applied to biopharmaceutical bioprocesses, and the economic metrics have greatly improved [33,35,65].

This article describes the process of intensifying the PEGylated recombinant AAT protein. As mentioned in the process description section (Section 2.1), two processes were modeled (process A: conventional process; process B: intensified process). Each process has three sections: the upstream, downstream, and PEGylation sections. Process intensification was applied to the upstream part, while the downstream and PEGylation sections were kept the same for both processes. Conventional process A has a conventional fed-batch N-production bioreaction that starts with a seed inoculum of  $0.2 \times 10^6$  cells/mL. Process intensification was applied to process B by having step changes in the N-1 seed bioreactor and N-production bioreactors, resulting in a much higher seed inoculum density (i.e.,  $8 \times 10^6$  cells/mL). In order to support the high cell seed density of the production bioreactor, changes were assumed in the N-1 bioreactor’s operation mode (i.e., perfusion bioreactor).

At first, a comparison of the cost evaluation of all three processes was performed for a base case annual production of 200 kg/year with a selling price of USD 500/g. The analysis indicates that the CAPEX of process A is estimated at USD 100 million, while for process B, the CAPEX was estimated to be USD 86 million, which represents a 14% reduction in this category. The OPEX for process A was estimated to be USD 79 million/year, while the OPEX for process B was estimated to be USD 72 million/year, which represents a drop of 9%. The total COGs of processes A and B were calculated to be USD 420.5/g and USD 378.3/g, of which the operating COGs were USD 387.6/g and USD 350.4/g, respectively. Under the assumptions of 15 years and a 7% interest rate, the net present value difference between intensified process B and conventional process A is USD 38 million. Our results are in agreement with the savings in COG reported when using N-1 perfusion as a means for process intensification for monoclonal antibody production [66].

Different approaches to process intensification in the upstream bioprocessing part, such as N-1 perfusion followed by a high-inoculation fed-batch, high-seed fed-batch production, and concentrated fed-batch production, have been utilized as means of process intensification [67]. Process intensification in the upstream section helps to increase the final titer or time savings per run, thus increasing the manufacturing capacity [68]. For example, Yang et al. showed that increasing the inoculum seed cell density from  $0.4 \times 10^6$  to  $10 \times 10^6$  cells/mL lowers the duration to achieve a 5 g/L titer from 17 days to only 12 days [69]. Furthermore, Stepper et al. showed that an intensified ultrahigh seed cell density fed-batch (seed density is  $10 \times 10^6$  cell/mL) was able to achieve a titer at roughly half the duration of a conventional fed-batch process inoculated with  $0.7 \times 10^6$  cells/mL [70]. Moreover, Schulze et al. showed that increasing the seed cell density from  $0.3 \times 10^6$  to  $5 \times 10^6$  was capable of increasing volumetric productivity by 45% due to a decrease of 30% in the process duration and a 13% increase in the cell-specific productivity [71].

On a cellular level, the specific production of lactate and ammonium is reduced in an intensified (ultrahigh seed density) fed-batch relative to the conventional fed-batch process,

as an intensified fed-batch is shifted to the late exponential phase initially compared to the early exponential phase indicated by the reduced specific glucose consumption rate [72,73]. However, metabolic activity for both processes converges as the culture moves through the stationary phase, as reported by Schulze et al. [71]. Xu et al. conducted process intensification by employing N-1 perfusion/enriched batch media and redesigning the basal/feed media in terms of amino acid content, glucose concentration, and osmolality for the production of four monoclonal antibodies. They found that upon media optimization, the titer increased for mAb2 due to having a higher viable cell density but with comparable cell-specific productivity, while the titer increase in mAb1 was a result of the increase in viable cell density and cell-specific productivity [29]. The existing studies show that process intensification is capable of increasing volumetric productivity by either increasing cell-specific productivity and viable cell density or by decreasing the less productive cell growth phase [28]. Increasing the viable seed cell density is achievable using the perfusion mode for N-1 bioreaction operation, as perfusion allows for the continuous addition of substrate and the removal of undesirable metabolites such as ammonium and lactate [74]. Moreover, cell-specific productivity can be modulated by adjusting concentrations of amino acids in the feed, supplementing cellular metabolites in the feed, or adjusting feeding strategies [75–77]. Since volumetric productivity is greatly enhanced in the intensified process (0.24 g AAT/L/day) relative to conventional process A (0.11 g AAT/L/day), a significant reduction in bioreactor size and seed expansion footprint shrinkage are observed. For example, process A has a single N-1 inoculation bioreactor and four N production bioreactors of 500 and 2000 L, respectively, whereas process B has two N-1 inoculation bioreactors (200 L) and two N production bioreactors (2000 L).

Figures 4 and 5 help visualize the breakdown of CAPEX and OPEX per section. Figure 4 shows that the contribution of the upstream section to the overall CAPEX is reduced from 56% in conventional process A to 48% in intensified process B. This means that a reduction in the upstream CAPEX of 26% is attainable. A similar observation can be found in the contribution of the upstream section to the overall OPEX as it decreases from 28% (process A) to 21% in the intensified process B (Figure 5). Moreover, intensification results in an upstream OPEX reduction of 32% for the intensified process B when compared to conventional process A. The detailed operation of COG for the upstream section per category is shown in Figure 6. The facility-dependent cost follows the same trend as CAPEX because it is highly dependent on the equipment cost, as observed by Ding et al. [33]. It decreases from USD 48/g (process A) to approximately USD 35/g (process B). Furthermore, material costs are heavily reduced due to a reduction in bioreactor size from the conventional process A (USD 40.7/g) to the intensified process B (USD 19.0/g). The material cost in the upstream section is dominated by the media (basal/feed) used in the production of the N-bioreactor. There is significant shrinkage in the bioreactor sizes as the process intensifies, moving from process A to process B. For example, the scale of the N-1 inoculation bioreactor in conventional process A is 500 L, while the volume of the N-1 inoculation bioreactor in intensified process B is 200 L. Moreover, the number of production bioreactors differs between the conventional process A and the intensified process B. Two production bioreactors are used in the intensified process B (2000 L), while four production bioreactors, each with 2000 L, are needed in the conventional process A. Altogether, this means that less media is needed in the production of AAT, and thus, the material cost is significantly reduced upon process intensification. It should be mentioned that having an N-1 bioreactor operating in perfusion mode in process B results in a higher contribution of materials (USD 0.28/g) to the operating COG relative to process A (USD 0.03/g) due to the greater consumption of media in the N-1 bioreactor. In support of our findings, Xu et al. observed an 8-fold increase in media cost when comparing a perfusion culture relative to a fed-batch culture [47]. Moreover, the contribution of labor (USD 2.1/g) to the COG at the N-1 bioreactor step is higher than that of conventional process A (USD 1.1/g).

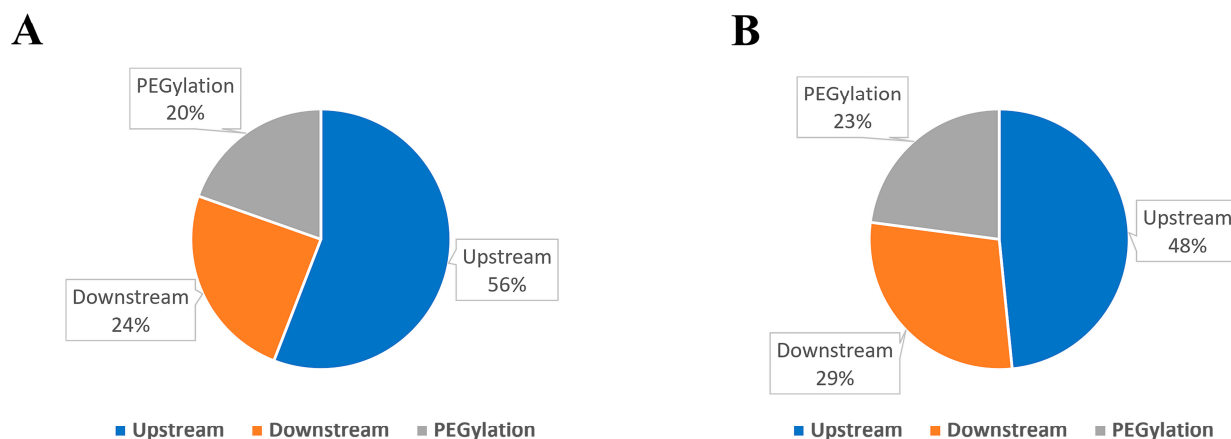


**Figure 4.** Capital cost (CAPEX) breakdown for all three processes in different sections of (A) conventional process A and (B) intensified process B.

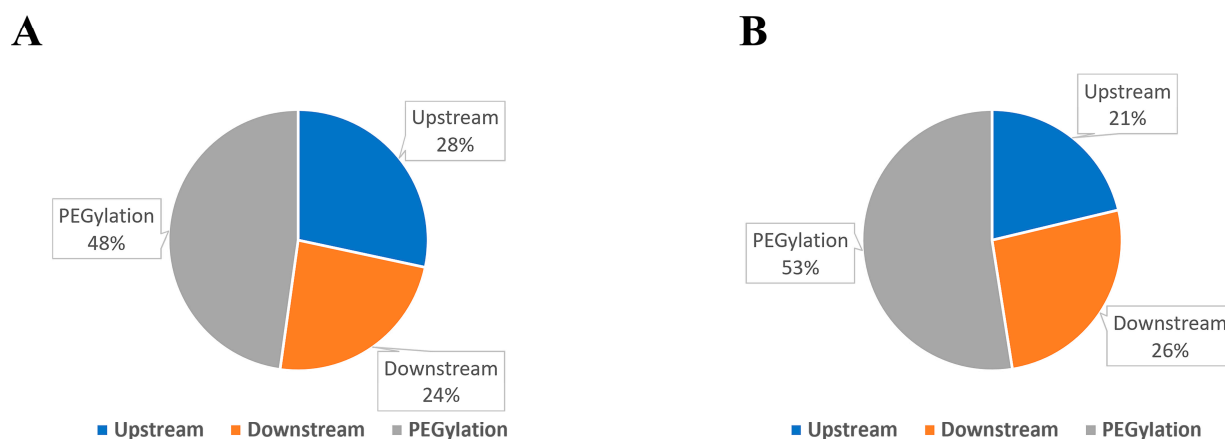


**Figure 5.** Operating cost expenditure (OPEX) breakdown for all three processes in different sections of (A) conventional process A and (B) intensified process B.

Although using perfusion mode in the production N-bioreactor is one strategy for achieving upstream intensification, a high seed cell density fed-batch N-production bioreactor was selected in our techno-economic model despite the findings that a fully continuous bioprocess has a lower cost of goods than a conventional bioprocess platform [78]. The reason for this is that the savings in manufacturing costs are captured in continuous downstream processing relative to conventional downstream processing, as demonstrated by Klutz et al. However, the trend is reversed when comparing fed-batch operations to continuous bioreactor operations [79]. The researchers compared the cost assessments for two different bioprocesses and found that cost savings are higher in the continuous downstream section than in the conventional downstream section. Moreover, they compared the specific COG for the upstream section of a conventional fed-batch bioreactor to a continuous perfusion bioreactor across a wide range of cell-specific productivities. They found that cell-specific productivity affects COG significantly, and fed-batch fermentation is more cost-efficient than perfusion fermentation at the same level of cell-specific productivity. This observation is corroborated by others as well [80].

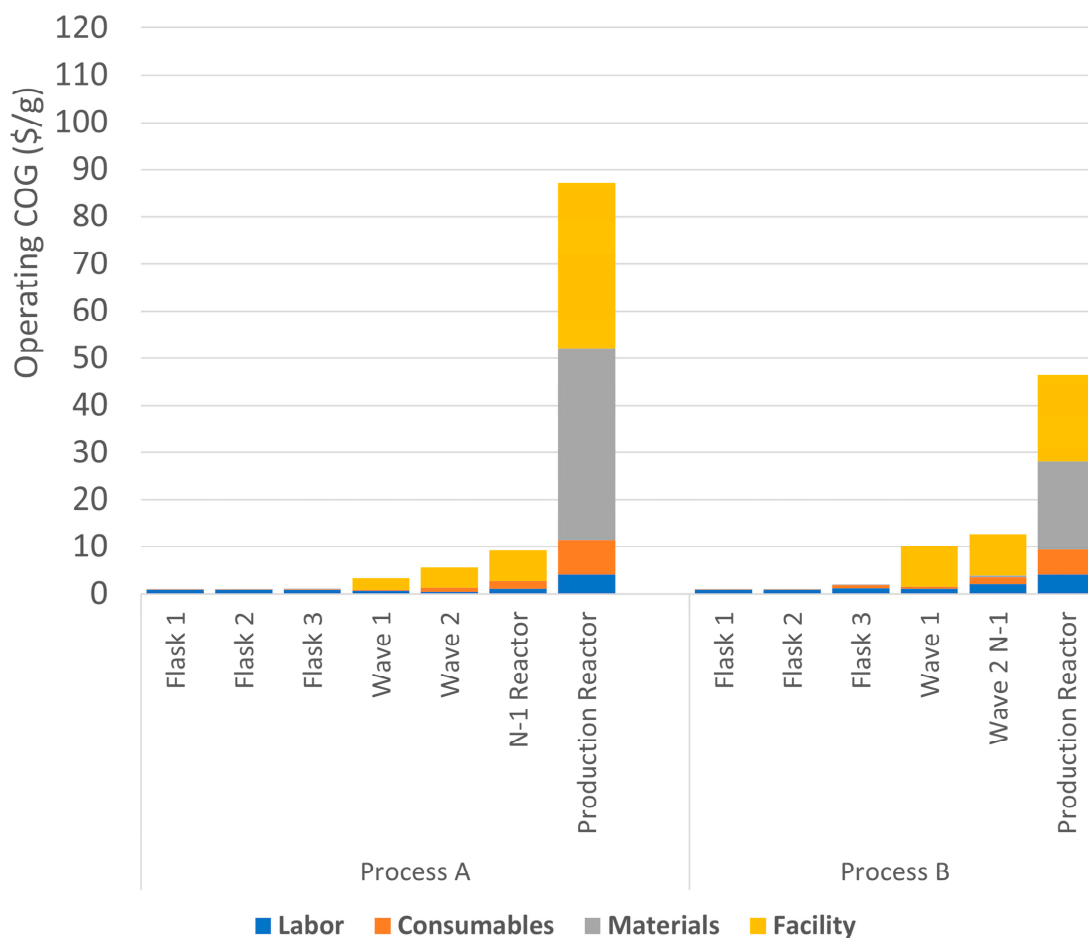


**Figure 6.** Detailed operating cost of goods for the upstream section per category for all three processes.

In order to understand the contribution of all unit operations to all sections in the cost of goods, waterfall diagrams were constructed for each process, showing the operating COG of each unit of operation according to its category (Figures 7 and 8). Figure 7 shows the waterfall diagram of the operating COG for the conventional process A. The main operating cost contributors are the N-production bioreactor (upstream, USD 87.3/g), capture affinity column (downstream, USD 57.9/g), and PEGylation reactor (PEGylation section, USD 167.8/g). As the operating COG for the N-production bioreactor is dominated by facility-dependent and material costs, the capture affinity column is dominated by consumables due to the high cost of affinity resin (USD 22.4/g) and material cost driven by the high consumption rate of the buffers, which results from the operation in bind-and-elute mode (27.8 USD/g), in line with the findings of Klutz et al. [79] and Hummel et al. [81]. On the other hand, the operating cost of the PEGylation reactor is highly driven by the cost of the PEG-maleimide reagent, resulting in a specific cost of goods of USD 161.3/g. It is worth noting that the absolute cost of goods for different unit operations in the downstream and PEGylation sections remains the same in process B because these sections were unchanged (Figure 8). Accordingly, Figure 8 shows a greater contribution of the capture affinity column and the PEGylation reactor in the operating COG for the intensified process.

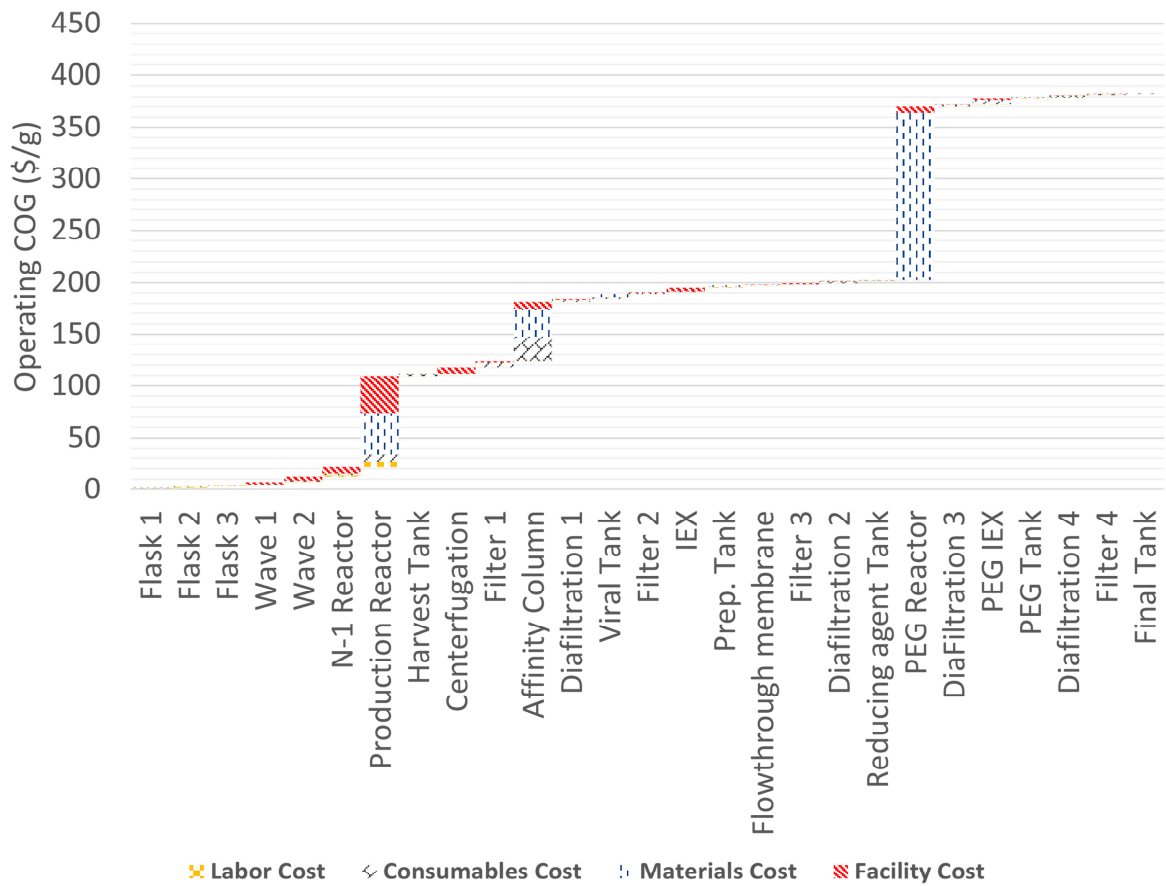


Figure 7. Waterfall diagram of the operating cost of goods for the conventional process A.

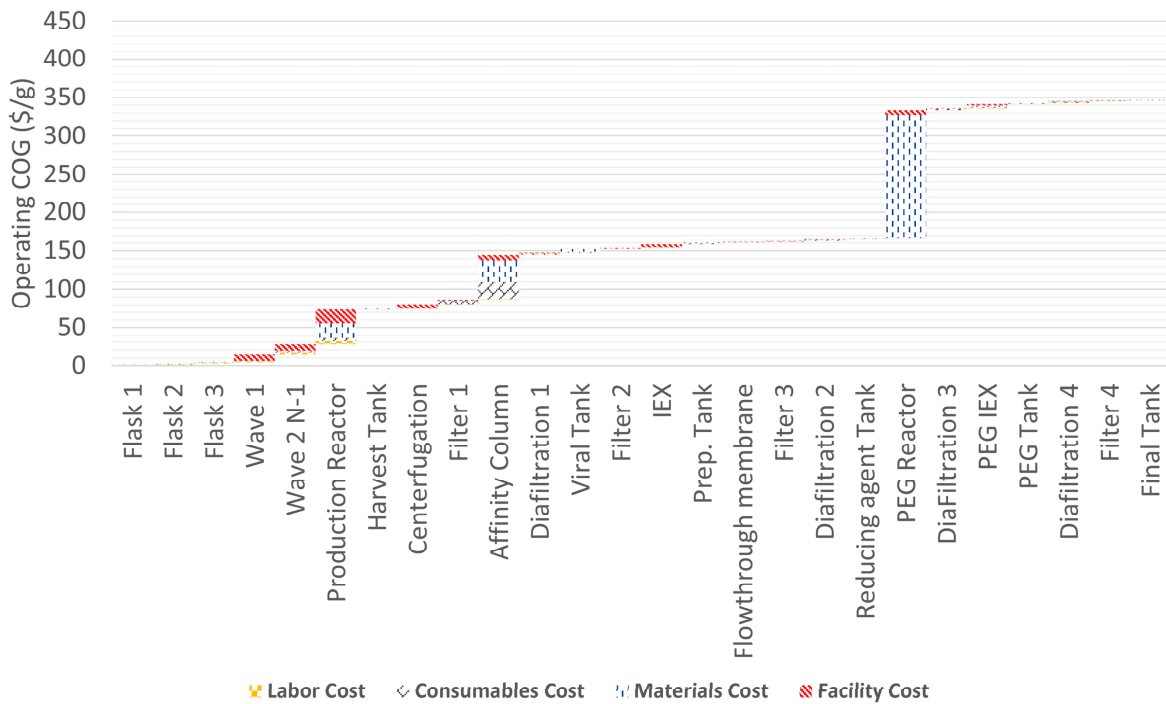


Figure 8. Waterfall diagram of the operating cost of goods for the intensified process B.

Protein PEGylation is one of the approaches to increasing the recombinant protein's half-life and making it comparable with the authentic human protein. Human authentic AAT is extensively sialylated with either diantennary disialylated or triantennary trisialylated glycans at positions Asn-46, Asn-83, and Asn-247 [82], and it is responsible for its long half-life in plasma. As stated earlier, the incomplete sialylation of recombinant protein produced in CHO cell culture derives from the need to assess other means of achieving a long circulation half-life. In this model, a 20 kDa PEG-maleimide was used for AAT conjugation to have a half-life comparable to that of the authentic AAT, as shown by Cantin et al. [83]. Despite the major contribution of the PEGylation section driven by the cost of the PEG-maleimide reagent and having other alternative approaches used for half-life extension, such as Fc-fusion, site-specific PEGylation was used in our model. Deveuve et al. evaluated the kinetics of hinge region cleavage in different classes of human monoclonal antibodies. Matrix metalloproteinase was used as a pathophysiological protease model. They found that the IgG1 hinge region was cleaved within 15 min of incubation at a ratio of 10 µg proteinase/50 µg IgG1 [84]. Moreover, matrix metalloproteinase was found to be elevated in the serum of COPD patients [85], which may raise the issue of the degradation of the Fc part. Furthermore, PEG conjugation to AAT confers stability against matrix metalloproteinases, which have been reported to digest authentic AAT [45].

### 3.2. Scenario Analysis

#### 3.2.1. Throughput Analysis

A scenario analysis was conducted to elucidate the technoeconomic impact of the varying performance parameters, including performance indicators (e.g., protein titer), critical quality attributes (e.g., product purity), and market parameters (e.g., yearly production level) [86]. Here, the influence of the yearly production level of PEG-AAT and the AAT titer in the N-production bioreactor was investigated based on the economics of the three processes.

A throughput analysis was used to evaluate the plant capacity effect on the economics of manufacturing PEG-AAT through a conventional process and intensified processes, as shown in Figures 9 and 10. Figure 9 shows that the cost of goods of PEG-AAT decreases as the throughput increases from 100 kg/year to 1000 kg/year for all processes. As shown in the figure, the decrease is slightly more pronounced in the intensified process B than in the conventional process A. This can be explained by the fact that an increase in throughput causes a non-uniform decrease in the specific operating cost of goods in the following order: downstream > upstream > PEGylation. Since the specific operating cost of goods in the upstream section has a greater contribution to the total COG in conventional process A than in intensified process B (Figures 4 and 5), the operating COG for process A is less sensitive to throughput increases than intensified process B. This happens as a result of increasing the contribution of the PEGylation section to the overall CAPEX and OPEX for the intensified process B. The capacity increase has little effect on the specific COG of the PEGylation section (Figure 10A), as this section is dominated by the specific cost of the materials that are not affected by the capacity increase. In our model, the unit prices of the materials were considered the same, as information about buying materials on different scales was not readily available.

On the other hand, a decrease in the specific operating COG for the upstream and downstream sections was observed for both processes. For example, the decrease ratios of the specific operating cost of goods in the upstream section were 17% and 21% for processes A and B, respectively, when the capacity was increased from 200 kg/year to 800 kg/year. Moreover, the decrease ratios of COG in the downstream section were 25% and 26% for processes A and B, respectively. Although the decreased ratio of the specific cost of goods of the upstream and downstream sections was around 20%, it did not cause a similar decrease in the total operating COG since the specific operating cost of goods for the PEGylation section became more dominant with an increase in the throughput. Figure 10B shows the detailed operating COG for all processes as a function of throughput increase.

The specific cost of labor and consumables and the facility-dependent cost all decrease with a capacity increase. The specific labor cost is inversely proportional to the capacity increase as the total labor cost is fixed [33,34]. Furthermore, the specific cost of consumables decreases as well, as there are savings in filters in the upstream and downstream sections. Moreover, facility-dependent costs decrease with an increase in throughput. Facility-dependent costs are highly dependent on capital investment. CAPEX increases are not exactly as linearly correlated as throughput increases are. Hence, savings of 35–40% in specific facility-dependent costs are observed for both processes as throughput increases.

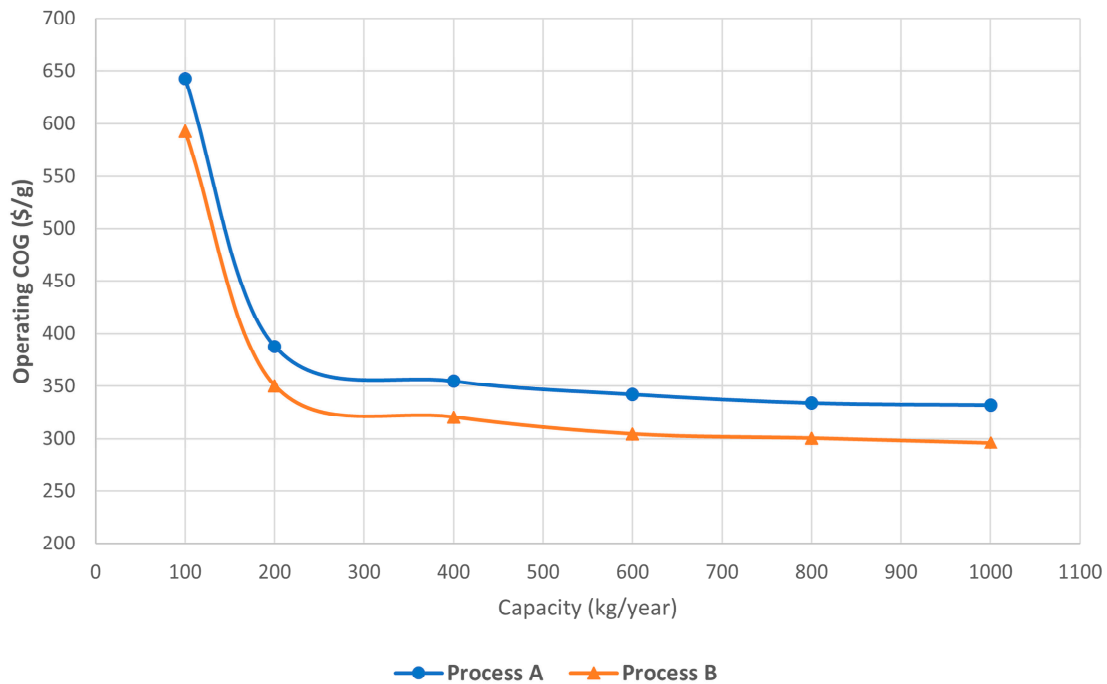


**Figure 9.** Overall throughput analysis comparing the operating-specific cost of goods for conventional process A and intensified process B.

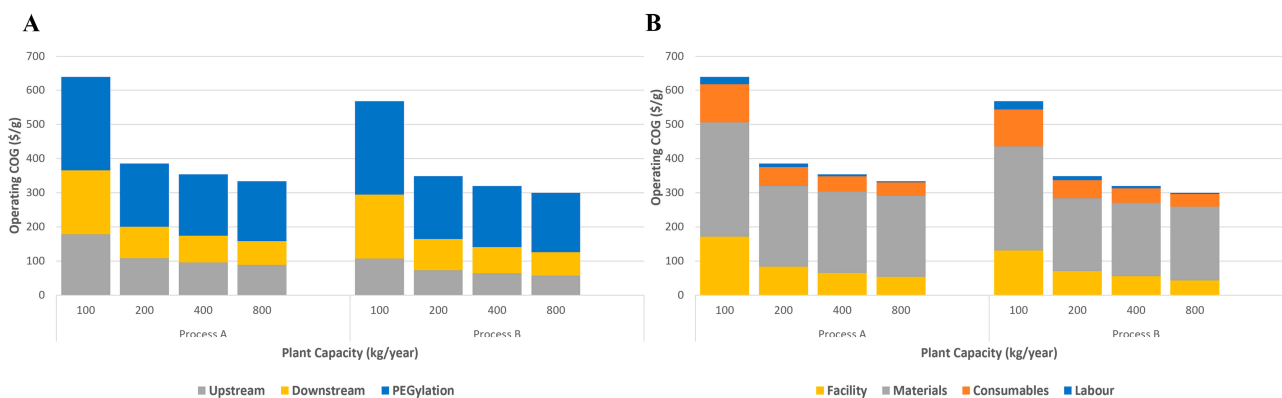


**Figure 10.** (A) Comparisons of the operating cost of goods are drawn per process section and (B) per category across a wide range of plant capacities for each process.

### 3.2.2. Upstream Titer

The upstream titer represents the concentration of recombinant parent AAT protein that is harvested from the bioreactor in each batch to be purified and PEGylated in the downstream and PEGylation sections, respectively. A sensitivity analysis was conducted by varying the cell-specific productivity for each process. The base-case cell-specific productivity of the conventional process A and the intensified processes B and C are mentioned in the

process description section. Here, the cell-specific productivity was increased for all processes from the base case (30 pg/cell/day) to the maximum theoretical 90 pg/cell/day [22].

Figure 11 presents the COG as a function of titer for all processes, showing that the conventional process A is more sensitive to titer increases than the intensified process B. Distinct sensitivity trends of the specific cost of goods with protein titers can be visualized. At low titer, the sensitivity is the greatest. As the titer increases, the sensitivity decreases significantly.

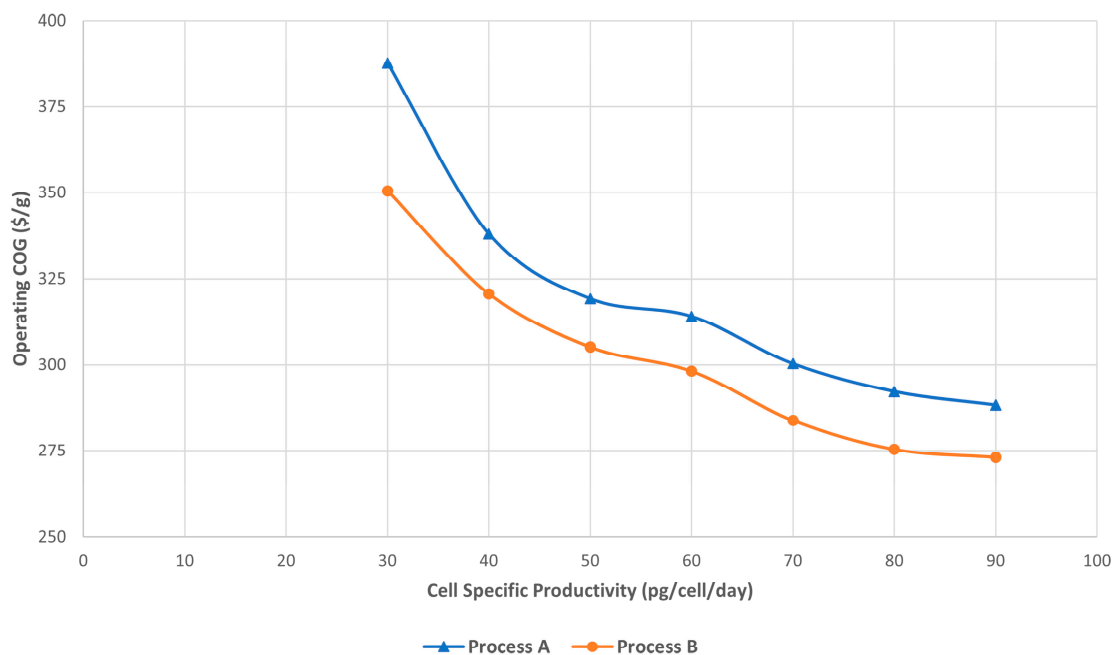


**Figure 11.** Operating cost of goods analysis as a function of protein titer for conventional process A and intensified process B.

It should be noted that the annual number of batches decreases for all processes as the production rate increases due to an increased batch time. The increase in batch time is due to the increase in the number of cyclic operations of chromatography columns in the downstream and PEGylation sections. For example, the number of cycles per batch of the capture affinity columns (process A) increases from 3 to 9 when the cell-specific productivity increases from the base case to the maximum theoretical 90 pg/cell/day due to the limited binding capacity of the resin.

To help visualize the reasons behind the decrease in the specific operating COG for process A, Figure 12A,B show the detailed operating COG across a wide range of cell-specific productivities per section of the process and per category for conventional process A. The cost of materials and consumables decreases with the increase in protein titer levels. In order to explain the decrease in the cost of materials and consumables in all sections of the process, a detailed explanation is helpful. In the upstream process, the use of materials and consumables (e.g., media and filters) is the same per batch. However, due to the decreased number of batches annually (i.e., larger batch size), the specific cost of materials and consumables in the upstream section decreases. On the other hand, fewer filters are used due to a decrease in the number of batches across the timeline of the facility operation with an increase in protein titer. Thus, the specific cost of consumables is reduced. It should be noted that the amount of capture affinity resin is roughly the same across different case scenarios of cell-specific productivities due to the same number of capture cycles annually. A similar observation can be made for the consumables in the PEGylation section as well, where their cost per batch increases with an increase in protein titer, but their specific cost decreases due to a smaller number of batches annually. Moreover, the cost of the PEG-maleimide reagent per batch increases with an increase in protein titer. However, the

specific cost of the PEG-maleimide reagent decreases due to a lower batch number annually. Thus, the cost of PEGylation, dominated by the cost of materials, decreases with an increase in productivity.

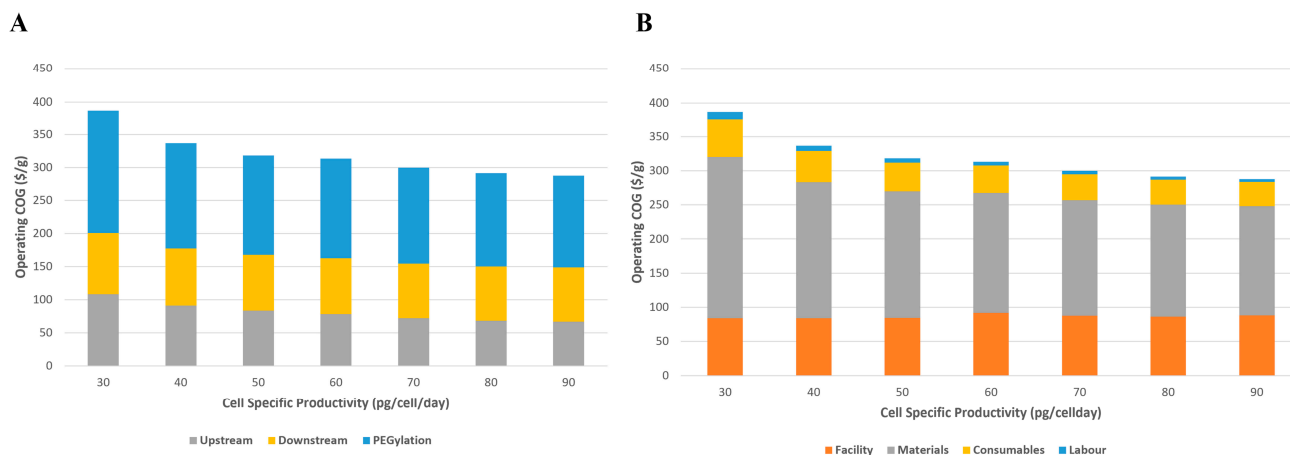


**Figure 12.** (A) Detailed breakdown of operating cost of goods for conventional process A per section and (B) category across a wide range of cell-specific productivities.

The total and specific facility-dependent cost is relatively the same for the upstream and downstream parts of the process across different protein titer levels. It should be noted that due to an increase in protein titer per batch, a second PEGylation reactor is used to meet the annual target of 200 kg. Hence, an increase in annual facility-dependent cost is observed when the cell-specific productivity reaches 60 pg/cell/day and beyond. Nonetheless, the specific facility-dependent cost is 5-fold lower than the specific cost of materials in this section, which means that the specific COG for the PEGylation section decreases with an increase in protein titer.

Figure 13 shows a comparison of the specific cost per category as a function of cell-specific productivity for both processes. Although the facility-dependent cost decreases as the CAPEX decreases for the intensified process B (i.e., a higher contribution of materials and consumables to the operating cost), the reduction percentage rate of consumables/materials is lower than that of the conventional process A. For example, the decrease in specific costs of materials and consumables for the intensified process B is 27% and 32%, respectively, when  $q_p$  is raised from 30 pg/cell/day to 90 pg/cell/day. On the other hand, the decreased percentages of the above-mentioned specific costs are 32% and 35% for conventional process A when  $q_p$  is raised from 30 pg/cell/day to 90 pg/cell/day. This can be explained by the greater specific cost of these two categories in the conventional process A, as process B causes a significant reduction in the specific cost of consumables and materials in the upstream part of the process. It should be noted that when comparing the conventional process A and intensified process B at the same protein titer level (i.e., conventional process A  $q_p = 70$  pg/cell/day and 90 pg/cell/day vs. intensified process B  $q_p = 30$  pg/cell/day and 40 pg/cell/day), a lower operating cost of goods is observed in the conventional process A, which can be explained by the larger batch size and lower number of batches annually, which result in a lower specific cost of the materials and consumables in the conventional process A.

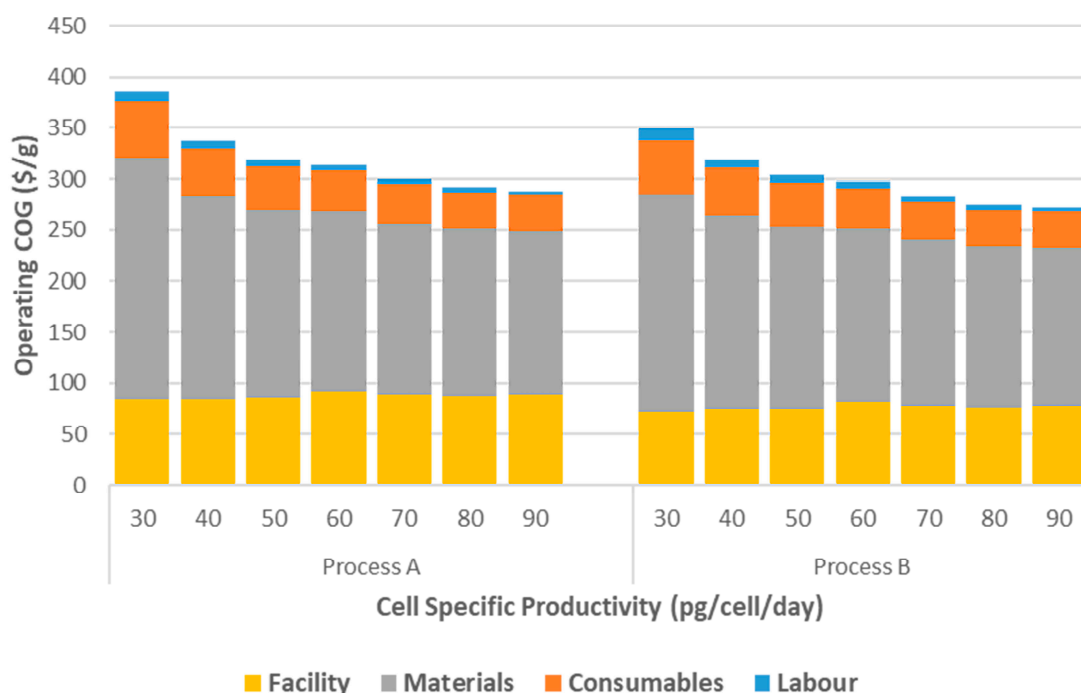


**Figure 13.** Comparison of operating-specific costs of goods per category between conventional process A and intensified process B.

#### 4. Conclusions

Process intensification results in improving the volumetric productivity of therapeutic proteins by either increasing the viable cell density in the production bioreactor, increasing the cell-specific productivity, or decreasing the non-productive phase in the production bioreactor. Here, a conventional process was designed to produce a PEGylated biopharmaceutical protein (AAT), and it was compared to an intensified process (process B). Process B uses an N-1 perfusion bioreactor. This causes a 40-fold increase in the inoculum cell seed density in process B compared to the conventional process A. The titer levels were calculated based on the assumptions mentioned in Table S1 and found to increase by 230% in the intensified process B compared to conventional process A. The total COGs of both processes were compared, and significant reductions in both CAPEX and OPEX were observed, especially in the upstream part of the process. A reduced footprint causes a reduction in CAPEX upon process intensification when comparing the conventional process A to the intensified process B. Moreover, a reduction is observed in the specific OPEX component costs (e.g., facility-dependent, material, and consumable costs) upon process intensification. Due to the significantly reduced bioreactor scales in the intensified process B, this leads to a reduction in media consumption in the N-production bioreactor and air filter sizes. Thus, a reduction in specific material and consumable costs is observed upon intensification. A scenario analysis was performed by varying the plant capacity from 100 kg/year to 1000 kg/year and the cell-specific productivity from the base case to the maximum theoretical 90 pg/cell/day. As the capacity increased, the specific cost of consumables and facility-dependent costs were reduced in all processes. On the contrary, the specific cost of materials was not different for all processes across the range of capacity. However, as the titer increased, the percentage reduction in the specific operating cost of goods differed among the two processes. While the specific costs of materials, consumables, and labor were reduced in the conventional process A with the titer increase, the percentage reduction in the specific operating cost of goods in the intensified process B was lower.

For future studies, process intensification approaches will be applied in the downstream and PEGylation sections to further reduce the total specific operating cost of goods. Using the continuous downstream section as part of the hybrid process helps to further

reduce the specific cost of consumables, materials, and facility-dependent costs in the downstream part. Furthermore, the process optimization of the PEGylation section is desired due to the high specific cost of materials in the PEGylation reactor.

**Supplementary Materials:** The following supporting information can be downloaded at: <https://www.mdpi.com/article/10.3390/pr12050979/s1>, Figure S1: Process flow diagram of intensified process B (upstream section). Figure S2: Equipment occupancy chart of the conventional process A. Figure S3: Gantt chart of the conventional process A. Figure S4: Equipment occupancy chart for intensified process B. Figure S5: Gantt chart of intensified process B. Table S1: Assumptions of the N production bioreactor in processes A and B. Table S2: Downstream and PEGylation unit operations yield.

**Author Contributions:** Conceptualization, S.A. and H.E.-T.; methodology, S.A.; software, S.A. and A.M.A.; validation, S.A. and A.M.A.; formal analysis, S.A. and A.M.A.; investigation, S.A. and A.M.A.; data curation, A.M.A.; writing—original draft preparation, S.A.; writing—review and editing, S.A., H.E.-T. and A.M.A.; supervision, S.A. and H.E.-T.; project administration, S.A.; funding acquisition, S.A. and H.E.-T. All authors have read and agreed to the published version of the manuscript.

**Funding:** This research was funded by the College of Graduate Studies, Kuwait University.

**Data Availability Statement:** The original contributions presented in the study are included in the article/Supplementary Materials. Further inquiries can be directed to the corresponding author (s.alkanaimsh@ku.edu.kw).

**Conflicts of Interest:** The authors declare no conflicts of interest. The funders had no role in the design of the study, in the collection, analysis, or interpretation of data, in the writing of the manuscript, or in the decision to publish the results.

## References

1. Lechowicz, U.; Rudzinski, S.; Jezela-Stanek, A.; Janciauskiene, S.; Chorostowska-Wynimko, J. Post-Translational Modifications of Circulating Alpha-1-Antitrypsin Protein. *Int. J. Mol. Sci.* **2020**, *21*, 9187. [[CrossRef](#)] [[PubMed](#)]
2. Viglio, S.; Iadarola, P.; D'Amato, M.; Stolk, J. Methods of Purification and Application Procedures of Alpha1 Antitrypsin: A Long-Lasting History. *Molecules* **2020**, *25*, 4014. [[CrossRef](#)] [[PubMed](#)]
3. Karatas, E.; Bouche-careilh, M. Alpha 1-Antitrypsin Deficiency: A Disorder of Proteostasis-Mediated Protein Folding and Trafficking Pathways. *Int. J. Mol. Sci.* **2020**, *21*, 1493. [[CrossRef](#)] [[PubMed](#)]
4. Marijanovic, E.M.; Fodor, J.; Riley, B.T.; Porebski, B.T.; Costa, M.G.S.; Kass, I.; Hoke, D.E.; McGowan, S.; Buckle, A.M. Reactive centre loop dynamics and serpin specificity. *Sci. Rep.* **2019**, *9*, 3870. [[CrossRef](#)] [[PubMed](#)]
5. McNulty, M.J.; Silberstein, D.Z.; Kuhn, B.T.; Padgett, H.S.; Nandi, S.; McDonald, K.A.; Cross, C.E. Alpha-1 antitrypsin deficiency and recombinant protein sources with focus on plant sources: Updates, challenges and perspectives. *Free Radic. Biol. Med.* **2021**, *163*, 10–30. [[CrossRef](#)]
6. Chung, H.-S.; Kim, J.-S.; Lee, S.M.; Park, S.J. Additional N-glycosylation in the N-terminal region of recombinant human alpha-1 antitrypsin enhances the circulatory half-life in Sprague-Dawley rats. *Glycoconj. J.* **2016**, *33*, 201–208. [[CrossRef](#)]
7. McElvaney, O.F.; Asakura, T.; Meinig, S.L.; Torres-Castillo, J.L.; Hagan, R.S.; Gabillard-Lefort, C.; Murphy, M.P.; Thorne, L.B.; Borczuk, A.; Reeves, E.P.; et al. Protease-anti-protease compartmentalization in SARS-CoV-2 ARDS: Therapeutic implications. *eBioMedicine* **2022**, *77*, 103894. [[CrossRef](#)]
8. Meyer, M.; Jaspers, I. Respiratory protease/antiprotease balance determines susceptibility to viral infection and can be modified by nutritional antioxidants. *Am. J. Physiol. Lung Cell. Mol. Physiol.* **2015**, *308*, L1189–L1201. [[CrossRef](#)]
9. Lomas, D.A. Does Protease-Antiprotease Imbalance Explain Chronic Obstructive Pulmonary Disease? *Ann. Am. Thorac. Soc.* **2016**, *13* (Suppl. S2), S130–S137.
10. Dey, T.; Kalita, J.; Weldon, S.; Taggart, C.C. Proteases and Their Inhibitors in Chronic Obstructive Pulmonary Disease. *J. Clin. Med.* **2018**, *7*, 244. [[CrossRef](#)]
11. O'Brien, M.E.; Murray, G.; Gogoi, D.; Yusuf, A.; McCarthy, C.; Wormald, M.R.; Casey, M.; Gabillard-Lefort, C.; McElvaney, N.G.; Reeves, E.P. A Review of Alpha-1 Antitrypsin Binding Partners for Immune Regulation and Potential Therapeutic Application. *Int. J. Mol. Sci.* **2022**, *23*, 2441. [[CrossRef](#)] [[PubMed](#)]
12. Crowther, D.C.; Belorgey, D.; Miranda, E.; Kinghorn, K.J.; Sharp, L.K.; Lomas, D.A. Practical genetics: Alpha-1-antitrypsin deficiency and the serpinopathies. *Eur. J. Hum. Genet.* **2004**, *12*, 167–172. [[CrossRef](#)] [[PubMed](#)]
13. Santos, G.; Turner, A.M. Alpha-1 antitrypsin deficiency: An update on clinical aspects of diagnosis and management. *Fac. Rev.* **2020**, *9*, 1. [[CrossRef](#)]
14. Kaplan, A.; Cosentino, L. Alpha1-antitrypsin deficiency: Forgotten etiology. *Can. Fam. Physician* **2010**, *56*, 19–24.

15. López-Campos, J.L.; Carrasco Hernandez, L.; Caballero Eraso, C. Implications of a Change of Paradigm in Alpha1 Antitrypsin Deficiency Augmentation Therapy: From Biochemical to Clinical Efficacy. *J. Clin. Med.* **2020**, *9*, 2526. [[CrossRef](#)] [[PubMed](#)]
16. Blanco, I.; Bueno, P.; Diego, I.; Pérez-Holanda, S.; Casas-Maldonado, F.; Esquinas, C.; Miravittles, M. Alpha-1 antitrypsin Pi\*Z gene frequency and Pi\*ZZ genotype numbers worldwide: An update. *Int. J. Chron. Obs. Pulmon. Dis.* **2017**, *12*, 561–569. [[CrossRef](#)]
17. McElvaney, O.F.; Fraughen, D.D.; McElvaney, O.J.; Carroll, T.P.; McElvaney, N.G. Alpha-1 antitrypsin deficiency: Current therapy and emerging targets. *Expert Rev. Respir. Med.* **2023**, *17*, 191–202. [[CrossRef](#)]
18. Bianchera, A.; Alomari, E.; Bruno, S. Augmentation Therapy with Alpha-1 Antitrypsin: Present and Future of Production, Formulation, and Delivery. *Curr. Med. Chem.* **2022**, *29*, 385–410. [[CrossRef](#)]
19. Edgar, R.G.; Patel, M.; Bayliss, S.; Crossley, D.; Sapey, E.; Turner, A.M. Treatment of lung disease in alpha-1 antitrypsin deficiency: A systematic review. *Int. J. Chron. Obs. Pulmon. Dis.* **2017**, *12*, 1295–1308. [[CrossRef](#)]
20. Smith, D.J.; Ellis, P.R.; Turner, A.M. Exacerbations of Lung Disease in Alpha-1 Antitrypsin Deficiency. *Chronic Obs. Pulm. Dis.* **2021**, *8*, 162–176. [[CrossRef](#)]
21. Li, W.; Fan, Z.; Lin, Y.; Wang, T.-Y. Serum-Free Medium for Recombinant Protein Expression in Chinese Hamster Ovary Cells. *Front. Bioeng. Biotechnol.* **2021**, *9*, 646363. [[CrossRef](#)] [[PubMed](#)]
22. Chin, C.L.; Chin, H.K.; Chin, C.S.H.; Lai, E.T.; Ng, S.K. Engineering selection stringency on expression vector for the production of recombinant human alpha1-antitrypsin using Chinese Hamster ovary cells. *BMC Biotechnol.* **2015**, *15*, 44. [[CrossRef](#)] [[PubMed](#)]
23. Koyuturk, I.; Kedia, S.; Robotham, A.; Star, A.; Brochu, D.; Sauvageau, J.; Kelly, J.; Gilbert, M.; Durocher, Y. High-level production of wild-type and oxidation-resistant recombinant alpha-1-antitrypsin in glycoengineered CHO cells. *Biotechnol. Bioeng.* **2022**, *119*, 2331–2344. [[CrossRef](#)] [[PubMed](#)]
24. Amann, T.; Hansen, A.H.; Kol, S.; Hansen, H.G.; Arnsdorf, J.; Nallapareddy, S.; Voldborg, B.; Lee, G.M.; Andersen, M.R.; Kildegaard, H.F. Glyco-engineered CHO cell lines producing alpha-1-antitrypsin and C1 esterase inhibitor with fully humanized N-glycosylation profiles. *Metab. Eng.* **2019**, *52*, 143–152. [[CrossRef](#)] [[PubMed](#)]
25. Lalonde, M.-E.; Koyuturk, I.; Brochu, D.; Jabbour, J.; Gilbert, M.; Durocher, Y. Production of  $\alpha$ 2,6-sialylated and non-fucosylated recombinant alpha-1-antitrypsin in CHO cells. *J. Biotechnol.* **2020**, *307*, 87–97. [[CrossRef](#)] [[PubMed](#)]
26. Mellahi, K.; Brochu, D.; Gilbert, M.; Perrier, M.; Ansorge, S.; Durocher, Y.; Henry, O. Assessment of fed-batch cultivation strategies for an inducible CHO cell line. *J. Biotechnol.* **2019**, *298*, 45–56. [[CrossRef](#)] [[PubMed](#)]
27. Särnlund, S.; Jiang, Y.; Chotteau, V. Process intensification to produce a difficult-to-express therapeutic enzyme by high cell density perfusion or enhanced fed-batch. *Biotechnol. Bioeng.* **2021**, *118*, 3533–3544. [[CrossRef](#)] [[PubMed](#)]
28. Chen, C.; Wong, H.E.; Goudar, C.T. Upstream process intensification and continuous manufacturing. *Curr. Opin. Chem. Eng.* **2018**, *22*, 191–198. [[CrossRef](#)]
29. Xu, J.; Rehmann, M.S.; Xu, M.; Zheng, S.; Hill, C.; He, Q.; Borys, M.C.; Li, Z.J. Development of an intensified fed-batch production platform with doubled titers using N-1 perfusion seed for cell culture manufacturing. *Bioresour. Bioprocess.* **2020**, *7*, 17. [[CrossRef](#)]
30. Xu, J.; Xu, X.; Huang, C.; Angelo, J.; Oliveira, C.L.; Xu, M.; Xu, X.; Temel, D.; Ding, J.; Ghose, S.; et al. Biomanufacturing evolution from conventional to intensified processes for productivity improvement: A case study. *MAbs* **2020**, *12*, 1770669. [[CrossRef](#)]
31. Müller, D.; Klein, L.; Lemke, J.; Schulze, M.; Kruse, T.; Saballus, M.; Matuszczyk, J.; Kampmann, M.; Zijlstra, G. Process intensification in the biopharma industry: Improving efficiency of protein manufacturing processes from development to production scale using synergistic approaches. *Chem. Eng. Process. Process Intensif.* **2022**, *171*, 108727. [[CrossRef](#)]
32. Pollock, J.; Coffman, J.; Ho, S.V.; Farid, S.S. Integrated continuous bioprocessing: Economic, operational, and environmental feasibility for clinical and commercial antibody manufacture. *Biotechnol. Prog.* **2017**, *33*, 854–866. [[CrossRef](#)] [[PubMed](#)]
33. Ding, C.; Ardeschna, H.; Gillespie, C.; Ierapetritou, M. Process design of a fully integrated continuous biopharmaceutical process using economic and ecological impact assessment. *Biotechnol. Bioeng.* **2022**, *119*, 3567–3583. [[CrossRef](#)] [[PubMed](#)]
34. Yang, O.; Prabhu, S.; Ierapetritou, M. Comparison between Batch and Continuous Monoclonal Antibody Production and Economic Analysis. *Ind. Eng. Chem. Res.* **2019**, *58*, 5851–5863. [[CrossRef](#)]
35. Mahal, H.; Branton, H.; Farid, S.S. End-to-end continuous bioprocessing: Impact on facility design, cost of goods, and cost of development for monoclonal antibodies. *Biotechnol. Bioeng.* **2021**, *118*, 3468–3485. [[CrossRef](#)] [[PubMed](#)]
36. Bas, M.; Terrier, A.; Jacque, E.; Dehenne, A.; Pochet-Béghin, V.; Béghin, C.; Dezetter, A.S.; Dupont, G.; Engrand, A.; Beaufile, B.; et al. Fc Sialylation Prolongs Serum Half-Life of Therapeutic Antibodies. *J. Immunol.* **2019**, *202*, 1582–1594. [[CrossRef](#)] [[PubMed](#)]
37. Ngantung, F.A.; Miller, P.G.; Brushett, F.R.; Tang, G.L.; Wang, D.I. RNA interference of sialidase improves glycoprotein sialic acid content consistency. *Biotechnol. Bioeng.* **2006**, *95*, 106–119. [[CrossRef](#)] [[PubMed](#)]
38. Raymond, C.; Robotham, A.; Spearman, M.; Butler, M.; Kelly, J.; Durocher, Y. Production of  $\alpha$ 2,6-sialylated IgG1 in CHO cells. *MAbs* **2015**, *7*, 571–583. [[CrossRef](#)] [[PubMed](#)]
39. Veronese, F.M.; Mero, A. The impact of PEGylation on biological therapies. *BioDrugs* **2008**, *22*, 315–329. [[CrossRef](#)]
40. Holz, E.; Darwish, M.; Tesar, D.B.; Shatz-Binder, W. A Review of Protein- and Peptide-Based Chemical Conjugates: Past, Present, and Future. *Pharmaceutics* **2023**, *15*, 600. [[CrossRef](#)]
41. Mao, L.; Russell, A.J.; Carmali, S. Moving Protein PEGylation from an Art to a Data Science. *Bioconjugate Chem.* **2022**, *33*, 1643–1653. [[CrossRef](#)]
42. Belén, L.H.; Rangel-Yagui, C.d.O.; Beltrán Lissabet, J.F.; Effer, B.; Lee-Estevez, M.; Pessoa, A.; Castillo, R.L.; Fariás, J.G. From Synthesis to Characterization of Site-Selective PEGylated Proteins. *Front. Pharmacol.* **2019**, *10*, 1450. [[CrossRef](#)]
43. Dozier, J.K.; Distefano, M.D. Site-specific PEGylation of therapeutic proteins. *Int. J. Mol. Sci.* **2015**, *16*, 25831–25864. [[CrossRef](#)]

44. Liu, X.; Vanvarenberg, K.; Kouassi, K.G.W.; Mahri, S.; Vanbever, R. Production and characterization of mono-PEGylated alpha-1 antitrypsin for augmentation therapy. *Int. J. Pharm.* **2022**, *612*, 121355. [[CrossRef](#)] [[PubMed](#)]
45. Liu, X.; Kouassi, K.G.W.; Vanbever, R.; Dumoulin, M. Impact of the PEG length and PEGylation site on the structural, thermodynamic, thermal, and proteolytic stability of mono-PEGylated alpha-1 antitrypsin. *Protein Sci.* **2022**, *31*, e4392. [[CrossRef](#)] [[PubMed](#)]
46. Zhu, W.; Li, L.; Deng, M.; Wang, B.; Li, M.; Ding, G.; Yang, Z.; Medynski, D.; Lin, X.; Ouyang, Y.; et al. Oxidation-resistant and thermostable forms of alpha-1 antitrypsin from Escherichia coli inclusion bodies. *FEBS Open Bio* **2018**, *8*, 1711–1721. [[CrossRef](#)]
47. Xu, S.; Gavin, J.; Jiang, R.; Chen, H. Bioreactor productivity and media cost comparison for different intensified cell culture processes. *Biotechnol. Prog.* **2017**, *33*, 867–878. [[CrossRef](#)] [[PubMed](#)]
48. Padawer, I.; Ling, W.L.W.; Bai, Y. Case Study: An accelerated 8-day monoclonal antibody production process based on high seeding densities. *Biotechnol. Prog.* **2013**, *29*, 829–832. [[CrossRef](#)]
49. Zhang, X.; Hou, Y.; Ding, X.; Ye, S.; Cao, H.; Wang, Z.; Du, X.; Xie, Y.W.; Li, C. Purification and analysis of human alpha1-antitrypsin concentrate by a new immunoaffinity chromatography. *Prep. Biochem. Biotechnol.* **2014**, *44*, 725–737. [[CrossRef](#)]
50. Stone, M.C.; Borman, J.; Ferreira, G.; Robbins, P.D. Effects of pH, conductivity, host cell protein, and DNA size distribution on DNA clearance in anion exchange chromatography media. *Biotechnol. Prog.* **2018**, *34*, 141–149. [[CrossRef](#)]
51. Fan, J.; Luo, J.; Song, W.; Chen, X.; Wan, Y. Directing membrane chromatography to manufacture  $\alpha$ 1-antitrypsin from human plasma fraction IV. *J. Chromatogr. A* **2015**, *1423*, 63–70. [[CrossRef](#)] [[PubMed](#)]
52. Shirataki, H.; Matsumoto, Y.; Konoike, F.; Yamamoto, S. Viral clearance in end-to-end integrated continuous process for mAb purification: Total flow-through integrated polishing on two columns connected to virus filtration. *Biotechnol. Bioeng.* **2023**, *120*, 2977–2988. [[CrossRef](#)] [[PubMed](#)]
53. Wang, X.-D.; Wei, N.-N.; Wang, S.-C.; Yuan, H.-L.; Zhang, F.-Y.; Xiu, Z.-L. Kinetic Optimization and Scale-Up of Site-Specific Thiol-PEGylation of Loxenatide from Laboratory to Pilot Scale. *Ind. Eng. Chem. Res.* **2018**, *57*, 14915–14925. [[CrossRef](#)]
54. Silberstein, D.Z.; Karuppanan, K.; Aung, H.H.; Chen, C.H.; Cross, C.E.; McDonald, K.A. An oxidation-resistant, recombinant alpha-1 antitrypsin produced in Nicotiana benthamiana. *Free Radic. Biol. Med.* **2018**, *120*, 303–310. [[CrossRef](#)] [[PubMed](#)]
55. Chohanadisai, W.; Huang, J.; Huang, N.; Lönnerdal, B. Stability of recombinant human alpha-1-antitrypsin produced in rice in infant formula. *J. Nutr. Biochem.* **2003**, *14*, 386–393. [[CrossRef](#)] [[PubMed](#)]
56. Conley, L.; Tao, Y.; Henry, A.; Koepf, E.; Cecchini, D.; Pieracci, J.; Ghose, S. Evaluation of eco-friendly zwitterionic detergents for enveloped virus inactivation. *Biotechnol. Bioeng.* **2017**, *114*, 813–820. [[CrossRef](#)] [[PubMed](#)]
57. Huangfu, C.; Zhang, J.; Ma, Y.; Jia, J.; Li, J.; Lv, M.; Ma, X.; Zhao, X.; Zhang, J. Large-scale purification of high purity  $\alpha$ 1-antitrypsin from Cohn Fraction IV with virus inactivation by solvent/detergent and dry-heat treatment. *Biotechnol. Appl. Biochem.* **2018**, *65*, 446–454. [[CrossRef](#)] [[PubMed](#)]
58. Shukla, A.A.; Jiang, C.; Ma, J.; Rubacha, M.; Flansburg, L.; Lee, S.S. Demonstration of robust host cell protein clearance in biopharmaceutical downstream processes. *Biotechnol. Prog.* **2008**, *24*, 615–622. [[CrossRef](#)] [[PubMed](#)]
59. Huang, J.; Sutliff, T.D.; Wu, L.; Nandi, S.; Bengel, K.; Terashima, M.; Ralston, A.H.; Drohan, W.; Huang, N.; Rodriguez, R.L. Expression and Purification of Functional Human  $\alpha$ -1-Antitrypsin from Cultured Plant Cells. *Biotechnol. Prog.* **2001**, *17*, 126–133. [[CrossRef](#)]
60. Sugiura, M.; Hayakawa, S.; Adachi, T.; Ito, Y.; Hirano, K.; Sawaki, S. A simple one-step purification of human  $\alpha$ 1-proteinase inhibitor by immunoabsorbent column chromatography. *J. Biochem. Biophys. Methods* **1981**, *5*, 243–249. [[CrossRef](#)]
61. Martínez-Jothar, L.; Doukeridou, S.; Schiffelers, R.M.; Sastre Torano, J.; Oliveira, S.; van Nostrum, C.F.; Hennink, W.E. Insights into maleimide-thiol conjugation chemistry: Conditions for efficient surface functionalization of nanoparticles for receptor targeting. *J. Control. Release* **2018**, *282*, 101–109. [[CrossRef](#)]
62. Boodhoo, K.V.K.; Flickinger, M.C.; Woodley, J.M.; Emanuelsson, E.A.C. Bioprocess intensification: A route to efficient and sustainable biocatalytic transformations for the future. *Chem. Eng. Process. Process Intensif.* **2022**, *172*, 108793. [[CrossRef](#)]
63. Scown, C.D.; Baral, N.R.; Yang, M.; Vora, N.; Huntington, T. Technoeconomic analysis for biofuels and bioproducts. *Curr. Opin. Biotechnol.* **2021**, *67*, 58–64. [[CrossRef](#)]
64. Chai, S.Y.W.; Phang, F.J.F.; Yeo, L.S.; Ngu, L.H.; How, B.S. Future era of techno-economic analysis: Insights from review. *Front. Sustain.* **2022**, *3*, 924047. [[CrossRef](#)]
65. Walther, J.; Godawat, R.; Hwang, C.; Abe, Y.; Sinclair, A.; Konstantinov, K. The business impact of an integrated continuous biomanufacturing platform for recombinant protein production. *J. Biotechnol.* **2015**, *213*, 3–12. [[CrossRef](#)] [[PubMed](#)]
66. Pohlscheidt, M.; Jacobs, M.; Wolf, S.; Thiele, J.; Jockwer, A.; Gabelsberger, J.; Jenzsch, M.; Tebbe, H.; Burg, J. Optimizing capacity utilization by large scale 3000 L perfusion in seed train bioreactors. *Biotechnol. Prog.* **2013**, *29*, 222–229. [[CrossRef](#)] [[PubMed](#)]
67. Müller, J.; Teale, M.; Steiner, S.; Junne, S.; Neubauer, P.; Eibl, D.; Eibl, R. Intensified and Continuous mAb Production with Single-Use Systems. In *Cell Culture Engineering and Technology: In Appreciation to Professor Mohamed Al-Rubeai*; Pörtner, R., Ed.; Springer International Publishing: Cham, Switzerland, 2021; pp. 401–429. [[CrossRef](#)]
68. Yang, W.C.; Minkler, D.F.; Kshirsagar, R.; Ryll, T.; Huang, Y.-M. Concentrated fed-batch cell culture increases manufacturing capacity without additional volumetric capacity. *J. Biotechnol.* **2016**, *217*, 1–11. [[CrossRef](#)]
69. Yang, W.C.; Lu, J.; Kwiatkowski, C.; Yuan, H.; Kshirsagar, R.; Ryll, T.; Huang, Y.-M. Perfusion seed cultures improve biopharmaceutical fed-batch production capacity and product quality. *Biotechnol. Prog.* **2014**, *30*, 616–625. [[CrossRef](#)]

70. Stepper, L.; Filser, F.A.; Fischer, S.; Schaub, J.; Gorr, I.; Voges, R. Pre-stage perfusion and ultra-high seeding cell density in CHO fed-batch culture: A case study for process intensification guided by systems biotechnology. *Bioprocess Biosyst. Eng.* **2020**, *43*, 1431–1443. [[CrossRef](#)]
71. Schulze, M.; Niemann, J.; Wijffels, R.H.; Matuszczyk, J.; Martens, D.E. Rapid intensification of an established CHO cell fed-batch process. *Biotechnol. Prog.* **2022**, *38*, e3213. [[CrossRef](#)]
72. Krumm, T.L.; Ehsani, A.; Schaub, J.; Stiefel, F. An Investigation into the Metabolic Differences between Conventional and High Seeding Density Fed-Batch Cell Cultures by Applying a Segmented Modeling Approach. *Processes* **2023**, *11*, 1094. [[CrossRef](#)]
73. Brunner, M.; Kolb, K.; Keitel, A.; Stiefel, F.; Wucherpennig, T.; Bechmann, J.; Unsoeld, A.; Schaub, J. Application of metabolic modeling for targeted optimization of high seeding density processes. *Biotechnol. Bioeng.* **2021**, *118*, 1793–1804. [[CrossRef](#)] [[PubMed](#)]
74. Kuiper, M.; Spencer, C.; Fäldt, E.; Vuillemez, A.; Holmes, W.; Samuelsson, T.; Gruber, D.; Castan, A. Repurposing fed-batch media and feeds for highly productive CHO perfusion processes. *Biotechnol. Prog.* **2019**, *35*, e2821. [[CrossRef](#)] [[PubMed](#)]
75. Xiao, S.; Ahmed, W.; Mohsin, A.; Guo, M. Continuous Feeding Reduces the Generation of Metabolic Byproducts and Increases Antibodies Expression in Chinese Hamster Ovary-K1 Cells. *Life* **2021**, *11*, 945. [[CrossRef](#)] [[PubMed](#)]
76. Ha, T.K.; Lee, G.M. Effect of glutamine substitution by TCA cycle intermediates on the production and sialylation of Fc-fusion protein in Chinese hamster ovary cell culture. *J. Biotechnol.* **2014**, *180*, 23–29. [[CrossRef](#)] [[PubMed](#)]
77. Torkashvand, F.; Vaziri, B.; Maleknia, S.; Heydari, A.; Vossoughi, M.; Davami, F.; Mahboudi, F. Designed Amino Acid Feed in Improvement of Production and Quality Targets of a Therapeutic Monoclonal Antibody. *PLoS ONE* **2015**, *10*, e0140597. [[CrossRef](#)]
78. Arnold, L.; Lee, K.; Rucker-Pezzini, J.; Lee, J.H. Implementation of Fully Integrated Continuous Antibody Processing: Effects on Productivity and COGm. *Biotechnol. J.* **2019**, *14*, 1800061. [[CrossRef](#)] [[PubMed](#)]
79. Klutz, S.; Holtmann, L.; Lobedann, M.; Schembecker, G. Cost evaluation of antibody production processes in different operation modes. *Chem. Eng. Sci.* **2016**, *141*, 63–74. [[CrossRef](#)]
80. Cataldo, A.L.; Burgstaller, D.; Hribar, G.; Jungbauer, A.; Satzer, P. Economics and ecology: Modelling of continuous primary recovery and capture scenarios for recombinant antibody production. *J. Biotechnol.* **2020**, *308*, 87–95. [[CrossRef](#)]
81. Hummel, J.; Pagkaliwangan, M.; Gjoka, X.; Davidovits, T.; Stock, R.; Ransohoff, T.; Gantier, R.; Schofield, M. Modeling the Downstream Processing of Monoclonal Antibodies Reveals Cost Advantages for Continuous Methods for a Broad Range of Manufacturing Scales. *Biotechnol. J.* **2019**, *14*, 1700665. [[CrossRef](#)]
82. Kolarich, D.; Weber, A.; Turecek, P.L.; Schwarz, H.P.; Altmann, F. Comprehensive glyco-proteomic analysis of human alpha1-antitrypsin and its charge isoforms. *Proteomics* **2006**, *6*, 3369–3380. [[CrossRef](#)] [[PubMed](#)]
83. Cantin, A.M.; Woods, D.E.; Cloutier, D.; Dufour, E.K.; Leduc, R. Polyethylene Glycol Conjugation at Cys232 Prolongs the Half-Life of  $\alpha 1$  Proteinase Inhibitor. *Am. J. Respir. Cell Mol. Biol.* **2002**, *27*, 659–665. [[CrossRef](#)] [[PubMed](#)]
84. Deveuve, Q.; Lajoie, L.; Barrault, B.; Thibault, G. The Proteolytic Cleavage of Therapeutic Monoclonal Antibody Hinge Region: More Than a Matter of Subclass. *Front. Immunol.* **2020**, *11*, 168. [[CrossRef](#)]
85. Mahor, D.; Kumari, V.; Vashisht, K.; Galgalekar, R.; Samarth, R.M.; Mishra, P.K.; Banerjee, N.; Dixit, R.; Saluja, R.; De, S.; et al. Elevated serum matrix metalloprotease (MMP-2) as a candidate biomarker for stable COPD. *BMC Pulm. Med.* **2020**, *20*, 302. [[CrossRef](#)] [[PubMed](#)]
86. McNulty, M.J.; Nandi, S.; McDonald, K.A. Technoeconomic Modeling and Simulation for Plant-Based Manufacturing of Recombinant Proteins. In *Recombinant Proteins in Plants: Methods and Protocols*; Schillberg, S., Spiegel, H., Eds.; Springer: New York, NY, USA, 2022; pp. 159–189. [[CrossRef](#)]

**Disclaimer/Publisher’s Note:** The statements, opinions and data contained in all publications are solely those of the individual author(s) and contributor(s) and not of MDPI and/or the editor(s). MDPI and/or the editor(s) disclaim responsibility for any injury to people or property resulting from any ideas, methods, instructions or products referred to in the content.